nature communications

Article

https://doi.org/10.1038/s41467-025-59956-z

A midbrain circuit mechanism for noise-induced negative valence coding

Received: 9 November 2024

Accepted: 6 May 2025

Published online: 17 May 2025

Check for updates

Siyao Zhou[1,2,3,9], Yuebin Zhu[1,2,3,9], Ana Du[1,2,3,9], Shuai Niu[1,2,3], Yonglan Du[1,2,3], Yan Yang[1], Wenqiang Chen[4,5], Siyu Du[1,2,3], Li Sun[1,2,3], Yijun Liu[1,2,3], Hangjun Wu[6], Huifang Lou[1,2,3], Xiao-Ming Li[3,7,8], Shumin Duan[1,2,3] & Hongbin Yang[1,2,3]

Unpleasant sounds elicit a range of negative emotional reactions, yet the underlying neural mechanisms remain largely unknown. Here we show that glutamatergic neurons in the central inferior colliculus (CIC^{glu}) relay noise information to GABAergic neurons in the ventral tegmental area (VTA^{GABA}) via the cuneiform nucleus (CnF), encoding negative emotions in mice. In contrast, the CIC^{glu}→medial geniculate (MG) canonical auditory pathway processes salient stimuli. By combining viral tracing, calcium imaging, and optrode recording, we demonstrate that the CnF acts downstream of CIC^{glu} to convey negative valence to the mesolimbic dopamine system by activating VTA^{GABA} neurons. Optogenetic or chemogenetic inhibition of any connection within the CIC^{glu}→CnF^{glu} → VTA^{GABA} circuit, or direct excitation of the mesolimbic dopamine (DA) system is sufficient to alleviate noise-induced negative emotion perception. Our findings highlight the significance of the CIC^{glu}→CnF^{glu} → VTA^{GABA} circuit in coping with acoustic stressors.

Sounds not only provide information about our surroundings but also evoke various emotional responses. In modern urban life, noise is a widespread and serious factor affecting human health. Clinical and animal studies have shown that unpleasant sounds can elicit negative emotions[1–5] and even pain[6–8], which can increase the risk of drug abuse[3]. While the neural pathways that transform auditory stimuli into salient actions have been extensively studied[9–12], the neural mechanisms that convert sounds into emotions remain unclear.

The inferior colliculus (IC), comprised of a central nucleus (CIC) and the surrounding shell nuclei (the dorsal cortex, DCIC; the external cortex, ECIC)[13], is the major auditory integration center in the midbrain. It plays a critical role in representing spectrotemporal features of sounds[14,15] and localizing sound sources[16]. Previous studies indicated that the DCIC and ECIC are the primary sites of non-auditory input to the IC, such as somatosensory inputs[17,18]. In contrast, the CIC is predominantly considered an auditory structure[19,20], indirectly relaying sound information to the auditory cortex through the medial geniculate (MG) nucleus[21,22]. We hypothesized that CIC neurons might also relay aversive sound information to the auditory cortex for negative emotion coding. However, we found that inhibition of the auditory cortex did not robustly alter acute noise-induced negative emotion responses or DA release in the nucleus accumbens (NAc). Using multidisciplinary approaches, we identified that CIC^{glu} neurons integrate multiple sensory information in an intensity-dependent manner and relay aversive

[1]Department of Neurobiology, Affiliated Mental Health Center & Hangzhou Seventh People's Hospital & Liangzhu Laboratory, Zhejiang University School of Medicine, Hangzhou, China. [2]MOE Frontier Science Center for Brain Science & Brain-Machine Integration, State Key Laboratory of Brain-machine Intelligence, School of Brain Science and Brain Medicine, Zhejiang University, Hangzhou, China. [3]NHC and CAMS Key Laboratory of Medical Neurobiology, Zhejiang University, Hangzhou, China. [4]Section of Integrative Physiology and Metabolism, Joslin Diabetes Center, Harvard Medical School, Boston, Massachusetts, USA. [5]Steno Diabetes Center Copenhagen, Herlev, Denmark. [6]Department of Pathology of Sir Run Run Shaw Hospital; Center of Cryo-Electron Microscopy, Zhejiang University, Hangzhou, China. [7]Department of Neurology of Second Affiliated Hospital and School of Brain Science and Brain Medicine, Zhejiang University School of Medicine, Hangzhou, China. [8]Nanhu Brain-Computer Interface Institute, Hangzhou, China. [9]These authors contributed equally: Siyao Zhou, Yuebin Zhu, Ana Du. e-mail: hongbinyang@zju.edu.cn

information to the cuneiform nucleus (CnF), which in turn, excites VTA^{GABA} neurons to encode negative valence. Therefore, our findings reveal a bottom-up mechanism for conveying unpleasant, stressful sound information to the mesolimbic DA system and encoding negative valence via a nociceptive pathway, providing a potential target for therapeutic intervention in motivation-related disorders, such as anxiety.

Results

Loud noise induces negative emotions and pain

To investigate the effect of noise on motivational behaviors, we exposed mice to various intensities of white noise (ambient noise at ~40 dB) using a closely positioned audio speaker. Compared to ~40 dB ambient noise or 50 dB white noise, 60 dB white noise elicited a weak aversion but did not affect anxiety-like behaviors (Fig. 1a–i). However, louder 80 dB white noise reliably induced both aversion and anxiety, while not significantly affecting locomotion in the open field test (OFT; Figs.1j, k). It did influence travel distance in the real-time place aversion test (RTCPA) as mice explored less on the side of the box where the louder sound was present (Fig.1b). In addition, while acute white noise stimulation did not affect the mechanical pain threshold (Figs. 1l–n), chronic exposure to 40 min of 80 dB noise reliably induced mechanical hypersensitivity (Figs. 1o–s). Together, these results indicate that 80 dB noise consistently alters mice's emotional states. Our next question is how loud noise conveys aversive information and affects animals' emotional states.

CIC^{glu} neurons integrate acoustic and nociceptive stimuli

Since loud noises contain both auditory and aversive information, we next explored the potential involvement of the CIC, a midbrain auditory structure, in processing aversive information beyond its role in integrating ascending auditory information. We performed c-fos immunostaining and observed, as expected, that 10 min of 80 dB noise stimulation induced a significant number of c-fos positive cells in the CIC (Supplementary Fig.1a, b). Interestingly, aversive stimuli from other sensory modalities also induced a large number of c-fos cells in the CIC (Supplementary Fig. 1c–e). These results suggest that CIC neurons are likely involved in processing aversive information rather than solely integrating auditory information. To further validate CIC responses to both acoustic and other aversive sensory stimuli, we utilized fiber photometry[23] to measure Ca^{2+} dynamics in CIC^{glu} neurons in response to various stimuli in head-fixed behaving mice, including white noise, noxious and innocuous stimuli (Supplementary Fig. 1f, g). We observed a pronounced increase in CIC^{glu} Ca^{2+} activity that was time-locked to the delivery of different intensity levels of white noise (Supplementary Fig. 1h–o). Additionally, aversive stimuli, such as electric shock (Supplementary Fig. 1p–r), tail pinch (Supplementary Fig. 1s–u), hot water, or cold water (Supplementary Fig. 1v), also increased CIC^{glu} Ca^{2+} activity, whereas sucrose reward decreased it (Supplementary Fig. 1w). The effects of tail brush and warm water (40 °C) were much weaker, if any (Supplementary Fig. 1s–v). Furthermore, the amplitude of CIC^{glu} Ca^{2+} activation in response to white

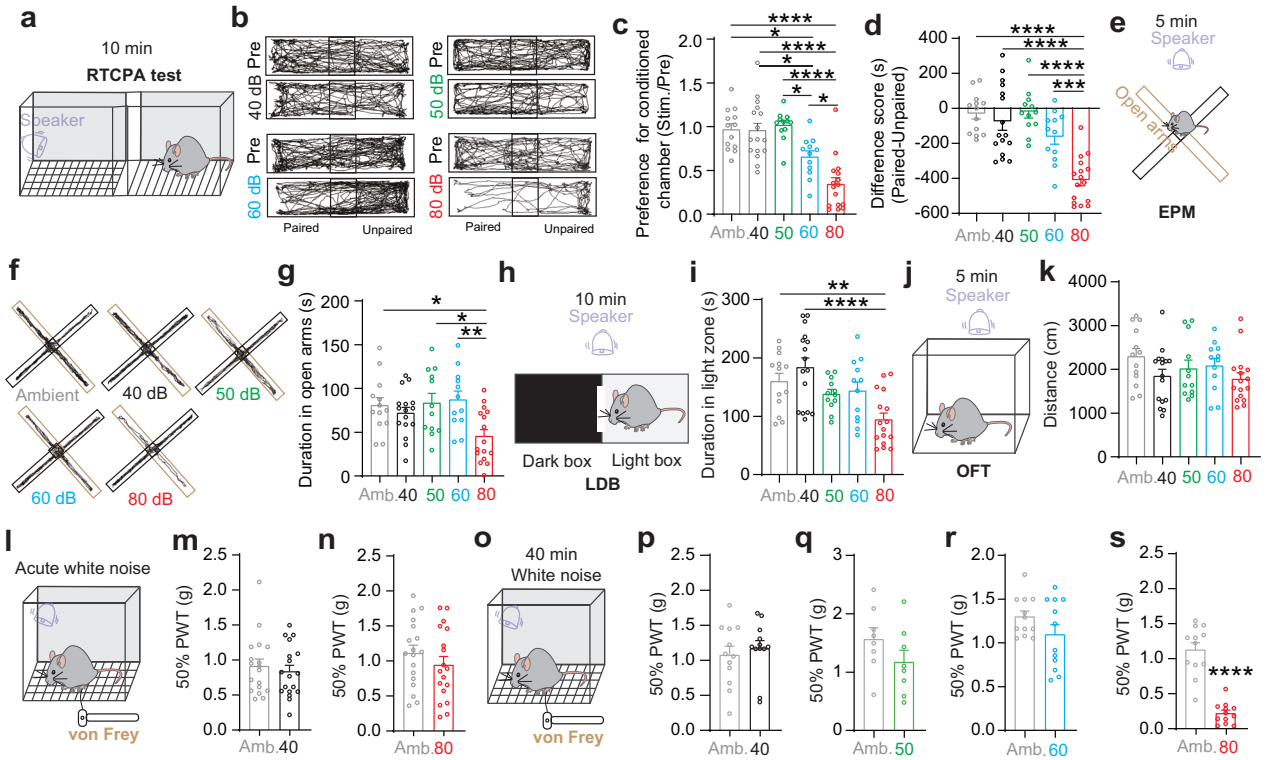

Fig. 1 | Noise-induced negative emotions. a Schematic of real-time conditional place aversion test (RTCPA) assays paired with 10 min sound stimulation. **b** Representative mouse traces in the RTCPA test with 40 dB, 50 dB, 60 dB, or 80 dB white noise exposure. **c** Preference score for white noise paired chamber ($n = 13, 16, 12, 12, 16$ mice for Ambient, 40-, 50-, 60-, 80-dB, respectively; one-way ANOVA with Tukey's post hoc test). **d** Difference score of performance across sound-paired chambers at varying decibel levels ($n = 13, 16, 12, 12, 16$ mice for Ambient, 40-, 50-, 60-, 80-dB, respectively; one-way ANOVA with Tukey's post hoc test). **e**, **f** Schematic and representative mouse traces in the elevated plus maze (EPM) under 5 min sound stimulation. **g** Time spent in the open arms ($n = 13, 16, 12, 12, 16$ mice for Ambient, 40-, 50-, 60-, 80-dB, respectively; one-way ANOVA with Tukey's post hoc test). **h** Experimental design for light-dark box (LDB) test under 10 min sound stimulation. **i** Time spent in the light zone ($n = 13, 16, 12, 12, 16$ mice for Ambient, 40-, 50-, 60-, 80-dB, respectively; one-way ANOVA with Tukey's post hoc test). **j** Open field test (OFT) under 5 min sound stimulation. **k** Travel distance ($n = 13, 16, 12, 12, 16$ mice for Ambient, 40-, 50-, 60-, 80-dB, respectively; one-way ANOVA with Tukey's post hoc test). **l** Experimental design for von Frey test. **m**, **n** 50% mechanical pain threshold (paw withdrawal threshold, PWT) under acute white noise ($n = 18$ mice, Paired t-test). **o**–**s** 50% mechanical pain threshold test after 40 min white noise stimulation (40 dB, 12 mice; 50 dB, 8 mice; 60 dB, 12 mice; 80 dB, 12 mice; Paired t-test). All graphs are represented as mean ± SEM. $^{*}p < 0.05$, $^{**}p < 0.01$, $^{***}p < 0.001$ or $^{****}p < 0.0001$.

noise, shock, or mechanical stimulation scaled with the intensity of the stimulus (Supplementary Fig. 1o, 1r, and 1u). These findings suggest that CIC^{glu} neurons not only responding to auditory stimuli but also bidirectionally to aversive and rewarding stimuli, independent of their sensory origin (Supplementary Fig. 1x).

Given that CIC^{glu} neurons are also involved in motor behavior[24], we next tested the possible involvement of locomotion in response to acoustic and aversive stimuli, which might confound the stimuli-evoked increases in CIC^{glu} Ca^{2+} activity. We sedated mice with 5% chloral hydrate, a sedative drug that does not block sensory information processing[25], and then delivered different intensity levels of white noise or electric shock. We observed that the CIC^{glu} neurons still reliably responded to white noise and aversive stimuli in a dose-dependent manner (Supplementary Fig. 2a–o), indicating that CIC^{glu} neurons integrate aversive stimuli across senses and that their activity is not solely driven by locomotor responses. In addition, using rabies-based retrograde trans-synaptic tracing, we found that CIC^{glu} neurons received inputs from nociceptive sensory-related brain regions (such as the lateral parabrachial nucleus, LPB[26,27]) in addition to inputs from predominantly auditory brain regions (Supplementary Fig. 2p–s). This could partially explain why CIC^{glu} neurons responded to nociceptive stimuli.

In contrast, GABAergic neurons in the CIC (CIC^{GABA}) were not activated during loud noise stimulation. However, in some animals, there was a substantial increase in activity after the loud noise stimulation (Supplementary Fig. 3a b). This variation may be attributed to the presence of distinct cell subtypes with different layers of CIC^{GABA} neurons[28]. Despite this, these neurons were inhibited by painful stimuli such as tail pinch (Supplementary Fig. 3c), and excited by reward, such as 5% sucrose (Supplementary Fig. 3d). These data suggest that CIC^{GABA} neurons are likely associated with encoding positive valence (Supplementary Fig. 3e). Consistent with this, optogenetic stimulation of CIC^{GABA} neurons promoted place preference (Supplementary Fig. 3f–h) without altering locomotion (Supplementary Fig. 3i). Additionally, stimulation of CIC^{GABA} neurons might promote exploratory behaviors (Supplementary Fig. 3j–l).

Next, we investigated whether individual CIC^{glu} neurons exhibit selectivity in response to unpleasant sounds and nociceptive stimuli. Since fiber photometry does not provide information about the activity of individual neurons, we used miniscope-based Ca^{2+} imaging to record the activity of individual cells through a GRIN lens implanted in the CIC of Vglut2-Cre mice expressing GCaMP6m while the animals were exposed to various sensory stimuli (Figs. 2a, b; and Supplementary Fig. 3m). We observed that the majority of CIC^{glu} neurons (~41–59%) were activated by 80 dB white noise or by noxious stimuli (shock, pinch, or hot water), although some neurons were inhibited by these stimuli (Figs. 2c–f). Furthermore, by tracking 78 cells that experienced all four types of stimuli, we found that 26% of these CIC^{glu} neurons responded to both loud white noise and one nociceptive stimulus (Fig. 2g). Together, these results reveal that individual CIC^{glu} neurons respond to a range of aversive sensory stimuli and exhibit a diverse response pattern.

To achieve better temporal resolution of CIC^{glu} neuron activity in response to various sensory stimuli, we performed in vivo optrode recordings to investigate whether any subpopulations of CIC^{glu} neurons selectively processed loud white noise stimulation (Figs. 2h, I; and Supplementary Fig. 3n). After identifying channelrhodopsin-2 (ChR2)-tagged CIC^{glu} neurons (Figs. 2j–l), we administered 80 dB white noise, tail pinch, and hot water to the mice. Although some CIC^{glu} neurons were inhibited by or did not respond to these stimuli, the majority of CIC^{glu} neurons (~70%) were excited by them (Figs. 2m–o). Moreover, among the 27 cells that were exposed to all three stimuli, 41% of them were excited by both 80 dB white noise and noxious stimuli (pinch and hot water) (Fig. 2p). These results further confirmed that many CIC^{glu} neurons are multifunctional, capable of integrating both auditory and aversive information.

In summary, these findings demonstrate that many CIC^{glu} neurons non-selectively process unpleasant sounds and aversive somatosensory stimuli, highlighting their role in encoding aversive information associated with loud noise.

CIC^{glu} neurons regulate sound-induced emotional responses

After establishing that CIC^{glu} neurons are activated by aversive stimuli, it remains to be determined whether this population is necessary or sufficient for gating behavioral responses to unpleasant stimuli. To address this, we conducted a series of optogenetic experiments to manipulate CIC^{glu} neurons bidirectionally (Supplementary Fig. 3o–v). The results showed that optogenetic inhibition of CIC^{glu} neurons did not alter locomotor activity (Supplementary Fig. 3p) or promote place preference (Supplementary Fig. 3q). However, this inhibition reliably reduced 80 dB noise-induced aversion (Figs. 2q–s), anxiety (Figs. 2t–v), and chronic 80 dB noise-induced mechanical hyperactivity (Fig. 2w). Conversely, optogenetic stimulation of CIC^{glu} neurons induced an avoidance response (Supplementary Fig. 3r–v). Taken together, these results demonstrate that CIC^{glu} neurons are both necessary and sufficient for encoding noise-induced negative emotions (Fig. 2x). The next question is: What are the downstream targets of CIC^{glu} neurons in the regulation of noise-induced perception of negative emotion?

CIC^{glu} neurons relay negative valence to CnF but not MG

Given that the medial geniculate (MG) nucleus acts as a relay center between the inferior colliculus and the auditory cortex[21,22], we first optogenetically activated the CIC^{glu} → MG pathway but did not induce aversion (Supplementary Fig. 4a–c). Furthermore, while CIC-targeted MG cells responded to white noise and painful stimuli during fiber photometry recording, these cells did not discriminate between different intensities of noise or aversive stimuli (Supplementary Fig. 4d–g). These data suggest that the CIC^{glu} → MG pathway may primarily encode salience rather than emotional valence.

To investigate additional downstream targets of CIC^{glu} neurons, we mapped the projections by injecting anterograde AAV-DIO-synaptophysin-mCherry into the CIC of Vglut2-Cre mice (Supplementary Fig. 4h). We observed dense projections from CIC^{glu} neurons in the MG, the anterior dorsal periaqueductal grey (adPAG), and the cuneiform nucleus (CnF), but not in the ventral tegmental area (VTA), the LPB (a nociceptive information transmission center), or lateral NAc (NAcLat; Supplementary Fig. 4i–k).

Previous research reported that CnF neurons respond to nociceptive stimuli[29]. Based on this, we reasoned that CIC^{glu} neurons might relay aversive information in noise to the CnF, thereby promoting negative emotion perception. We first examined the functional synaptic connectivity between CIC^{glu} neurons and CnF neurons and confirmed that CIC^{glu} neurons form strong excitatory synaptic connections with CnF neurons but not with LPB neurons (Supplementary Fig. 4l–o; TTX and 4-AP in the recording solution). To further validate that CIC^{glu} neurons encode aversion through the CnF, we optogenetically stimulated CIC^{glu} terminals in the CnF, which significantly increased aversive responses (Supplementary Fig. 5a–e), similar to the effects observed when stimulating CIC^{glu} cell bodies (Supplementary Fig. 3r–v).

To further confirm that glutamatergic neurons in the CnF (CnF^{glu}) are downstream targets of CIC^{glu} neurons, we induced apoptosis in CnF^{glu} neurons by unilaterally injecting AAV-DIO-Caspase 3 into the CnF of Vglut2-Cre mice, along with Cre-dependent AAV-ChR2 into the ipsilateral CIC and implanted an optical fiber above the ipsilateral CIC of the same animal. Control animals received injections of AAV carrying Cre-dependent mCherry instead of caspase 3 into CnF, while all

https://doi.org/10.1038/s41467-025-59956-z

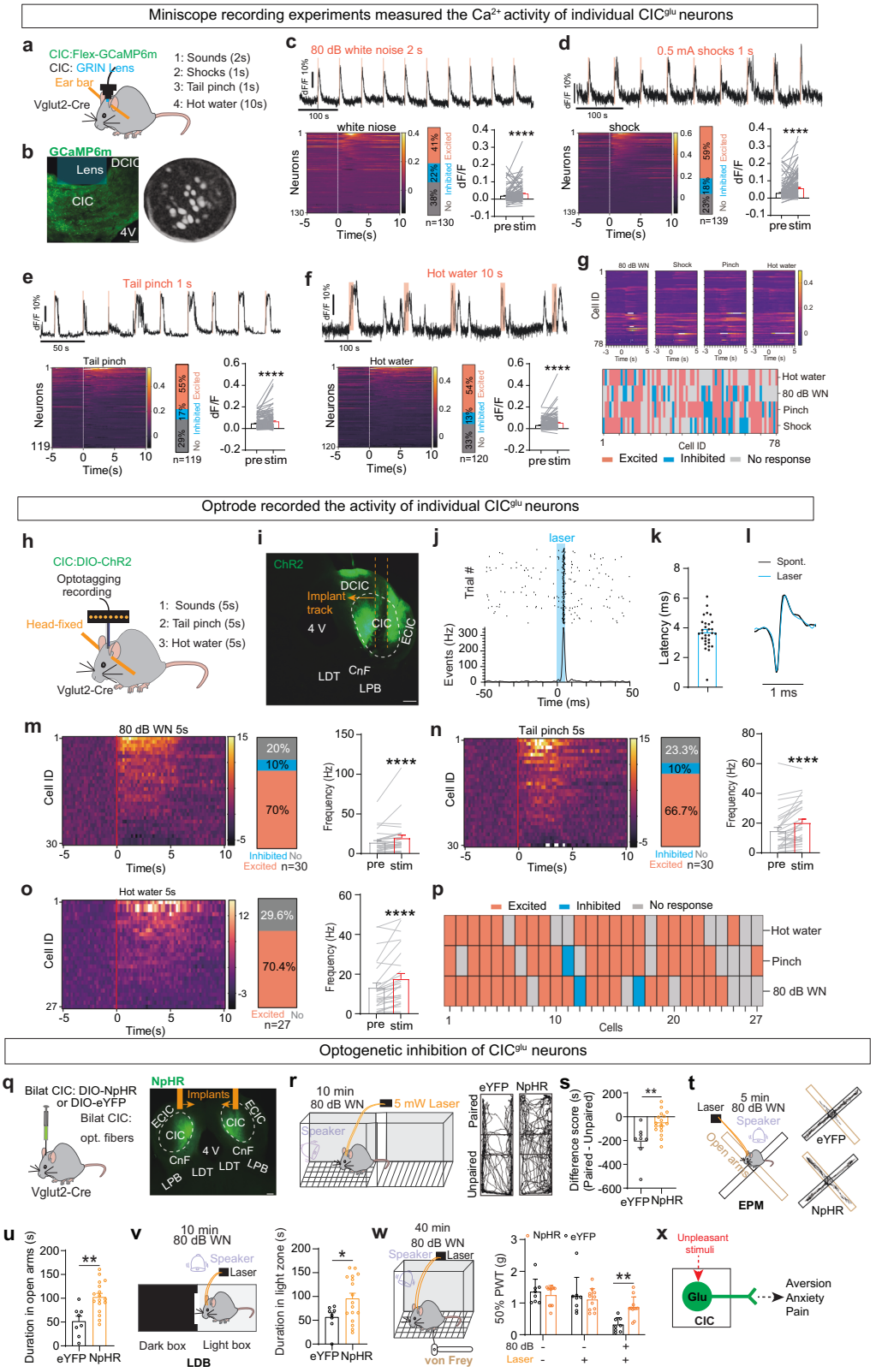

other procedures were identical (Supplementary Fig. 5f). Compared to control mice, optogenetic stimulation of CIC^{glu} neurons failed to induce an aversive response in mice where CnF^{glu} cells were ablated by caspase 3 injection (Supplementary Fig. 5g, h). Additionally, we found that CIC^{glu} neurons strongly project to the anterodorsal PAG (adPAG) but not the ventral PAG (Supplementary Fig. 4i). Although stimulation of the CIC^{glu}-PAG pathway induced a freezing-like behavior but not a classic avoidance (Supplementary Fig. 5i, k), aversive noise still could affect NAcLat DA release through this pathway. To explore this further, we optogenetically stimulated the CIC^{glu}-PAG pathway and found that this manipulation had a weak effect on NAcLat DA release (Supplementary Fig. 5l). Thus, noise-induced aversive responses result, at least in part, from activating the CIC^{glu}-CnF pathway.

Fig. 2 | CIC^{glu} neurons integrate multiple sensory information. **a** Experimental design. **b** Lens implanted in the CIC; scale bar, 100 μm. **c**–**f** Representative Ca^{2+} traces of excited neurons in response to 80 dB white noise (**c**), 0.5 mA shocks (**d**), tail pinch (**e**), and hot water (**f**). And all recorded neurons that exhibited significantly excited, inhibited, or no response Ca^{2+} activity before (pre) and during (stim) various stimuli (**c**)130 cells; d:139 cells; e:119 cells; f:120 cells; from 6 mice, Wilcoxon test). **g** Stimulus-specific responses in individual CIC^{glu} neurons while mice were exposed to different stimuli (top panel). (Bottom) each column represents the same neuron responding to these stimuli ($n = 78$ cells from 6 mice). **h** Experimental design. **i** Optrode implanted in CIC (scale bar, 200 μm). **j** The latency of light-evoked spikes relative to laser pulses (5 ms, blue; top) and corresponding spike firing frequency (bottom). **k** Mean latency to laser stimulation for ChR2-tagged neurons ($n = 30$ neurons from 3 mice). **l** Sample waveform for light-evoked (blue) and spontaneous (black) firing. **m** Hot map for spontaneous firing spikes from ChR2-tagged neurons in response to sound stimulation; pie graph shows the proportion of excited (light red), inhibited (blue) or no response (grey) ChR2-tagged cells in response to 80 dB white noise ($n = 30$ cells); (Right) mean firing frequency ($n = 30$ cells, Wilcoxon test). **n**, **o** Same as in (**m**) but for pinch (**n**, $n = 30$ cells) or heat (**o**, $n = 27$ cells). **p** Stimulus-specific responses in individual ChR2-tagged neurons while mice were exposed to different stimuli ($n = 27$ cells from 3 mice). **q** Implant locations (scale bar, 100 μm). **r** Representative trajectories in RTCPA test. **s** Difference score (NpHR: 17 mice, eYFP: 8 mice, Unpaired t-test). **t** Representative a path of eYFP- or NpHR-expressing mice during the EPM test. **u** Time spent in open arms and (**v**) Time spent in the light zone (NpHR: 17 mice, eYFP: 8 mice, Unpaired t-test). **w** 50% PWT (NpHR: 11 mice, eYFP: 8 mice, Two-way ANOVA with Holm-Sidak's post hoc test). **x** Experimental model. All graphs are represented as mean ± SEM. $^{*}p < 0.05$, $^{**}p < 0.01$ or $^{****}p < 0.0001$.

Since CIC^{glu} neurons responded to all intensities of white noise stimulation (Supplementary Fig. 1), we hypothesized that the CnF might selectively filter and process aversive sound information. To test this hypothesis, we utilized fiber photometry to record the activity of CIC-targeted CnF neurons in response to various intensities of white noise and painful stimuli (Supplementary Fig. 5m). Indeed, CIC-targeted CnF neurons responded to loud noise in a dose-dependent manner but did not respond to noise below 60 dB (Supplementary Fig. 5n–u). Additionally, these neurons also responded to high-intensity nociceptive stimuli (Supplementary Fig. 5v–y), suggesting that the CIC^{glu}→CnF^{glu} circuit processes painful information in addition to aversive sound information, thereby ruling out the possibility that CnF acts solely as an auditory filter. Furthermore, our retrograde tracing experiment demonstrated that about 10% of CnF-projecting CIC^{glu} cells have collateral projections to the MG, suggesting that some CnF-projecting CIC^{glu} neurons might relay the same stimulation to the MG as well. However, most of the cells projecting to these two brain regions are separate populations within the CIC (Supplementary Fig. 5z).

Together, those results suggest that CIC^{glu} neurons encode noise-induced negative emotions, at least in part, through the CIC^{glu}→CnF^{glu} circuit.

The CnF gates negative stimuli from CIC to VTA^{GABA} neurons

Given that unpleasant sound-induced negative emotional states might be associated with decreased DA in the NAc[3,30] and that local inhibition in the VTA significantly impacts the activity of DA neurons and aversive responses[31–34], we hypothesized that the CIC indirectly relays aversive sound information to VTA^{GABA} neurons to inhibit VTA^{DA} neurons (Supplementary Fig. 6a). To test this hypothesis, we used AAV1-Cre to anterogradely label the postsynaptic neurons of the CIC. Consistent with the results from AAV-DIO-synaptophysin-mCherry projection (Supplementary Fig. 4), the anterograde trans-synaptic AAV1-Cre labeled cells from the CIC were primarily located in the CnF, but not in the LPB or the VTA (Fig. 3a, b). This suggests that CIC neurons directly target the CnF, but not the VTA or the LPB (Fig. 3c). We also injected retrograde AAV2-Cre into the VTA of Ai14 reporter mice and observed that many retro-AAV2 labeled cells located in the CnF but not in the CIC (Fig. 3d, e). This result confirmed that the VTA directly receives inputs from the CnF but not from the CIC (Fig. 3f).

Notably, most of the anterogradely labeled cells in the VTA from the CnF were tyrosine hydroxylase (TH) immunonegative (99%, Figs. 3g, h), while the majority were GAD67 positive (64.3%, Figs. 3i, j), indicating that CnF^{glu} neurons selectively relay information to VTA^{GABA} neurons. We further confirmed that CnF^{glu} neurons preferentially form synaptic connections with VTA^{GABA} neurons but not VTA^{DA} neurons, using patch-clamp recording (Figs. 3k–m; TTX and 4-AP in the recording solution). In addition, we observed dense CnF^{GABA} projections in the red nucleus but not in the VTA, which excluded the possibility that CnF^{GABA} neurons directly inhibit VTA^{DA} neurons (Figs. 3n–p).

These results suggest that the CnF might act as a relay station of sensory information, connecting CIC^{glu} neurons to VTA^{GABA} neurons. Furthermore, we found that optogenetic activation of both CIC cell bodies and CIC neuronal terminals in the CnF resulted in a time-locked increase in VTA^{GABA} Ca^{2+} activity (Figs. 3q–r; Supplementary Fig. 6b, c), but a decrease in VTA^{DA} Ca^{2+} activity (Figs. 3s, t; and Supplementary Fig. 6d–e) and NAcLat DA release (Figs. 3u–v).

Together, these data suggest that CIC^{glu} neurons indirectly inhibit VTA^{DA} neurons by activating VTA^{GABA} neurons through CnF^{glu} neurons, at least in part (Fig. 3w).

Blocking the CIC^{glu}→CnF^{glu} → VTA^{GABA} circuit can effectively prevent noise-inducing negative emotions

The above results suggest that VTA^{GABA} neurons regulate noise-induced negative valence coding. To verify that VTA^{GABA} neurons respond to white noise stimulation, we injected AAV-Flex-GCaMP6m and implanted an optical fiber into the VTA of Vgat-Cre mice (Fig. 4a). We observed that VTA^{GABA} neurons responded to loud noise in a dose-dependent manner, whereas noise below 50 dB had a weak effect, if any (Figs. 4b–i). More importantly, chemogenetic inhibition of VTA^{GABA} neurons reliably prevented negative emotional responses induced by 80 dB noise (Figs. 4j–q; and Supplementary Fig. 6f–h) and the associated reduction in NAcLat DA levels (Figs. 4r–u). These experiments demonstrate that VTA^{GABA} neurons are involved in encoding unpleasant sound-induced negative emotions.

To further validate whether CIC^{glu} neurons encode sound aversion through the CnF^{glu} → VTA^{GABA} pathway, we performed optogenetic and chemogenetic inhibition of CnF-projecting CIC^{glu} neurons, VTA-projecting CnF^{glu} neurons, or CnF-targeted VTA cells during 80 dB noise stimulation (Fig. 5a–r; Supplementary Fig. 6i–j). We found that all these manipulations reliably prevented noise-induced aversion, anxiety, and pain (Figs. 5a–r). We next used an INTRSECT system[35] to specifically inhibit CnF neurons that receive CIC inputs and project to the VTA (Fig. 5s). As expected, selective silencing of the CIC→CnF→VTA pathway effectively reduced 80 dB white noise-induced negative emotions (Figs. 5t–x). Additionally, given that AAV1 can occasionally retrogradely travel to presynaptic neurons, though rarely[36], we excluded the potential impact of this on our experimental results using histological analysis (Supplementary Fig. 6k–o). Thus, these results suggest that the CIC^{glu}→CnF^{glu} → VTA^{GABA} circuit is crucial for encoding noise-induced negative emotions.

Auditory cortex in acute noise-induced NAc DA inhibition and negative emotions

Although the CIC^{glu} → MG pathway primarily responded to salience stimuli and MG neurons do not directly interact with the VTA (Supplementary Fig. 7a–d), the CIC^{glu} → MG pathway might relay noise information to the auditory cortex to encode negative emotions. To test this possibility, we used inhibitory (hM4Di) DREADDs (designer receptors exclusively activated by designer drugs) to bilaterally inhibit

https://doi.org/10.1038/s41467-025-59956-z

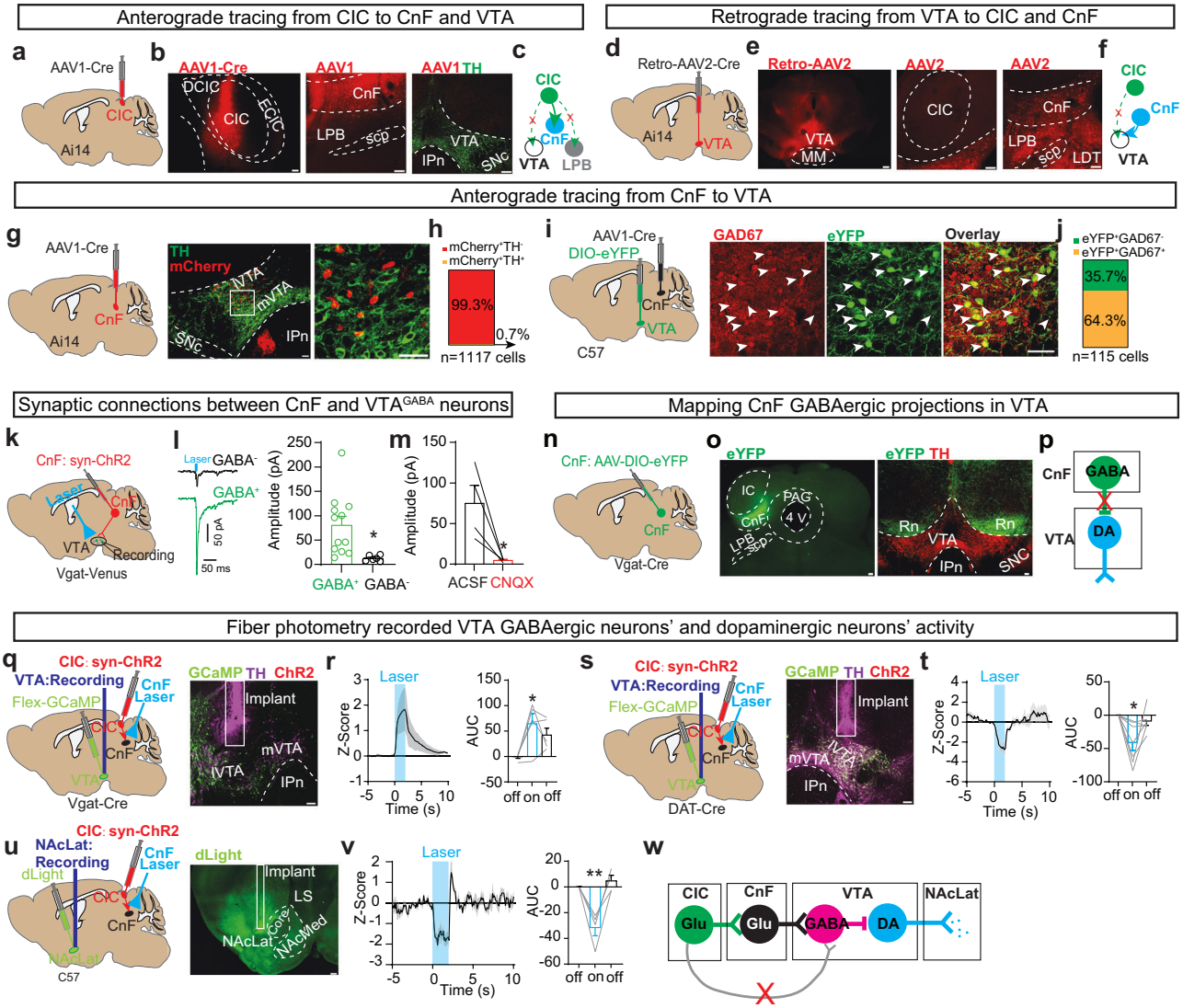

Fig. 3 | CnF bridges CIC^{glu} neurons and VTA^{GABA} neurons. **a** Experimental design. **b** AAV1-Cre injection in the CIC (left) and (middle) AAV1-labeled cells (red) in the CnF but not in the LPB and VTA (right; TH$^+$ cells, green), scale bar, 100 μm; the experiment was repeated 3 times from 3 mice. **c** Experimental model. **d** Experimental design. **e** RetroAAV2 injection site (left) and retroAAV2 labeled cells in the CnF (right) but not the CIC (middle; scale bar, 100 μm); the experiment was repeated 2 times from 2 mice. **f** Experimental model. **g** AAV1-Cre labeled cells (red) in VTA were TH-immunonegative (green) (scale bar, 50 μm). **h** Quantification of anterogradely labeled cells in VTA for TH-immunopositive, $n = 1117$ cells from 3 mice. **i** Anterograde labeled cells (green) in the VTA from CnF were GAD67 immunopositive (red), scale bar, 50 μm. **j** Quantification of anterogradely labeled cells in VTA for GAD67-immunopositive, $n = 115$ cells from 4 mice. **k** Experimental design. **l** Sample traces showing light-evoked EPSCs recorded in GABA-positive and GABA-negative neurons (left). EPSC amplitudes (right; GABA$^+$:12 cells; GABA$^-$:6 cells. Unpaired t-test). **m** Mean EPSC amplitudes ($n = 4$ neurons, Paired t-test). **n** Experimental design. **o** Left, AAV-DIO-eYFP injection site (scale bar, 100 μm). Right, representative fluorescent image showing CnF^{GABA} projections in the red nucleus (Rn) but not in the VTA (TH, red; scale bar, 100 μm). **p** Experimental model. **q** Schematic diagram. GCaMP6m expression (green) and optical fiber implanted site (scale bar, 100 μm). **r** Z-score of VTA^{GABA} neurons in response to 20 Hz optogenetic stimulation of ChR2-projections from the CIC in the CnF (left). (Right) comparison of mean AUC ($n = 5$ mice, one-way ANOVA with Tukey's post hoc test). **s**, **t** Similar to in (**q**, **r**) but for recording VTA^{DA} neurons ($n = 7$ mice, one-way ANOVA with Tukey's post hoc test). **u** Schematic diagram. dLight expression (green) and location of optical fiber track in the NAcLat (scale bar, 100 μm). **v** Z score for the NAcLat dopamine release (left; $n = 4$ mice). (Right) comparison of mean AUC ($n = 4$ mice, one-way ANOVA with Tukey's post hoc test). **w** Experimental model. All graphs are represented as mean ± SEM. $^*p < 0.05$ or $^{**}p < 0.01$.

the auditory cortex and examined the NAcLat DA release and behavioral responses during 80 dB noise stimulation. Intriguingly, inhibition of the auditory cortex did not significantly affect noise-induced NAcLat DA reduction or negative emotions (Supplementary Fig. 7e–j). Taken together, these data suggest that acute loud sounds lead to mesolimbic DA inhibition and negative emotional responses, potentially through the activation of VTA^{GABA} neurons by the CIC^{glu}→CnF^{glu} circuit, and may be independent of the top-down control[37]. However, we cannot exclude the possibility that top-down control could be involved in chronic noise-induced behavioral responses.

Exciting NAcLat DA activity reliably alleviates noise-induced negative emotional responses

Previous evidence suggests that lateral VTA (lVTA) DA neurons projecting to the NAcLat encode positive motivational valence[38,39]. Additionally, aversive stimulation decreases lVTA DA neuronal activity[40,41], and inhibition of NAcLat DA activity directly elicits aversive responses[42]. Activation of DA neurons is critical for preventing generalized anxiety[43]. Therefore, we reasoned that the negative emotional behaviors induced by intense white noise might be associated, at least in part, with a reduction in NAcLat DA activity. To test this hypothesis,

https://doi.org/10.1038/s41467-025-59956-z

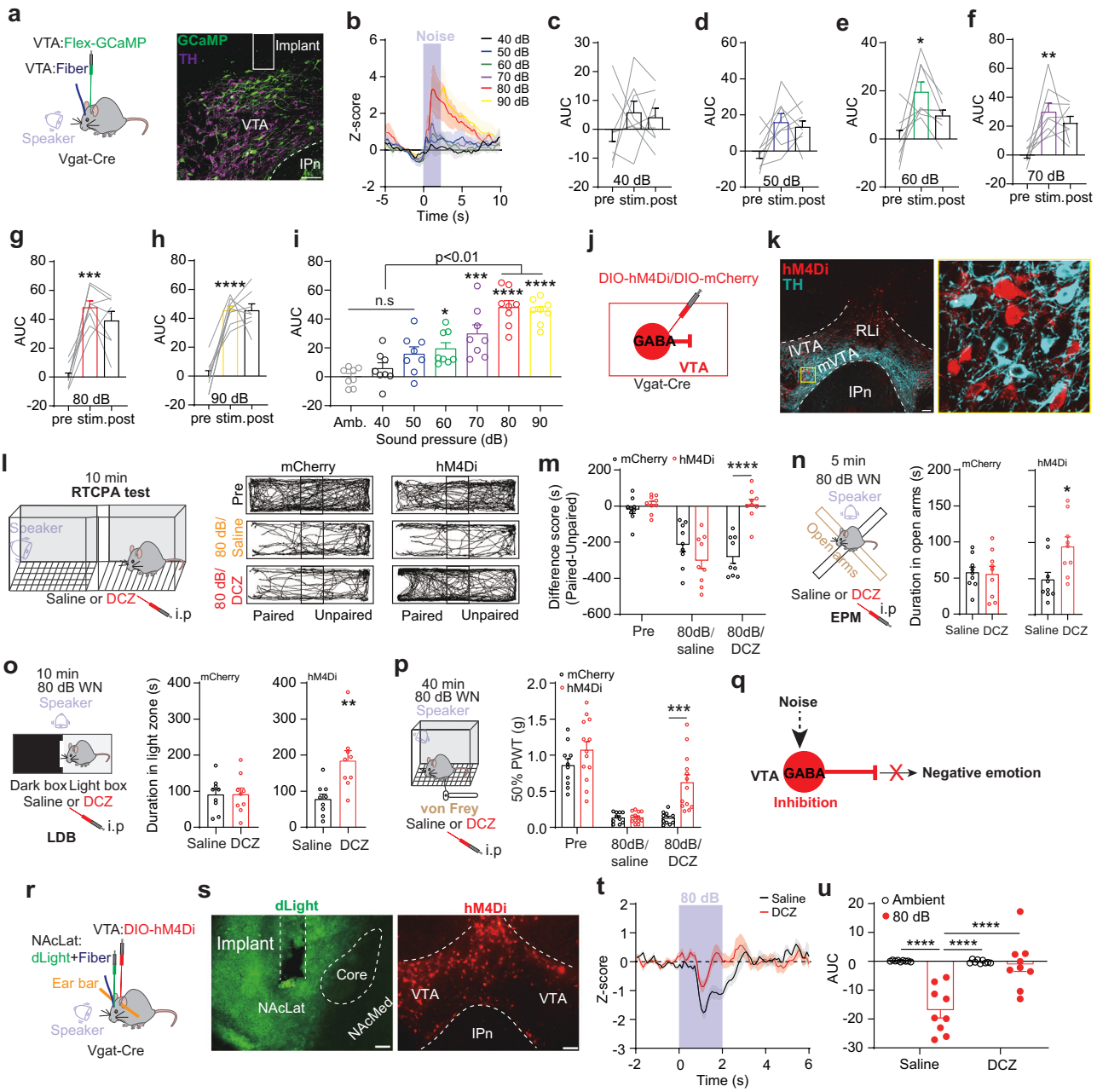

Fig. 4 | VTA^{GABA} neurons gate noise-induced negative emotion perception. **a** Left, experimental design. Right, GCaMP6m-expression in VTA^{GABA} neurons (green) and TH-immunopositive cells (purple) in the VTA (scale bar, 100 μm). **b** Z-score averages for VTA^{GABA} neurons in response to various decibels of white noise stimuli (duration, 2 s), $n = 8$ mice. **c**–**h** Fiber photometry recording for VTA^{GABA} neurons in response to 40 dB (**c**), 50 dB (**d**), 60 dB (e), 70 dB (**f**), 80 dB (**g**), and 90 dB (**h**) white noise stimulation, $n = 8$ mice, one-way ANOVA with Tukey's post hoc test. **i** Comparison of mean AUC during stimulation (2 s), $n = 8$ mice, one-way ANOVA with Tukey's post hoc test. **j** Experimental design. **k** Coronal brain slice image showing hM4Di-expression in the VTA^{GABA} neurons (red) and TH-immunopositive (cyan) cells in the VTA (scale bar, 100 μm). Yellow square showing zoomed-in view. **l** Schematic of RTCPA test (left). (Right) representative trajectories of mCherry- or hM4Di-expressing mouse exposed to 80 dB white noise stimulation after intraperitoneal (i.p) injection of saline or DCZ (100 μg/kg). **m** Difference score ($n = 9$ mice, Two-way ANOVA with HolmSidak's post hoc test). **n** Left, experimental design for EPM test. Right, time spent in open arms after saline or DCZ injection in mCherry-expressing and hM4Di-expressing mice ($n = 9$ mice, Unpaired t-test). **o** Left, experimental design. Right, time spent in light-box after saline or DCZ injection in mCherry- or hM4Di-expressing mice ($n = 9$ mice, Unpaired t-test). **p** 50% PWT test ($n = 10$–13 mice, Two-way ANOVA with HolmSidak's post hoc test). **q** Schematic of the experimental result. **r** Experimental design. **s** Coronal brain slice images showing dLight and optical fiber in the NAcLat and hM4Di-expression in the VTA^{GABA} neurons (red) in the VTA (scale bar, 100 μm). **t** Comparison of mean dLight responses in the NAcLat in response to 80 dB white noise stimulation in VTA^{GABA}-hM4Di mice treated with saline or DCZ (100 μg/kg, i.p). **u** Comparison of mean AUC from (**t**), $n = 9$ mice, one-way ANOVA with Tukey's post hoc test. All graphs are represented as mean ± SEM. $^{*}p < 0.05$, $^{**}p < 0.01$, $^{***}p < 0.001$ or $^{****}p < 0.0001$.

we injected DA sensors (dLight or DA3m) into the dorsal striatum, prefrontal cortex, and subregions of NAc (Supplementary Fig. 7k) to investigate which dopamine pathways are involved in sound-induced negative emotions. We observed that 60 or 80-dB white noise reliably decreased DA release in the NAcLat but did not significantly affect DA release in the dorsal striatum or PFC (Figs. 6a–h). Intriguingly, while ventral nucleus accumbens medial shell (vNAcMed) DA responds to aversive stimuli[40], we did not observe an increase in DA release in the

https://doi.org/10.1038/s41467-025-59956-z

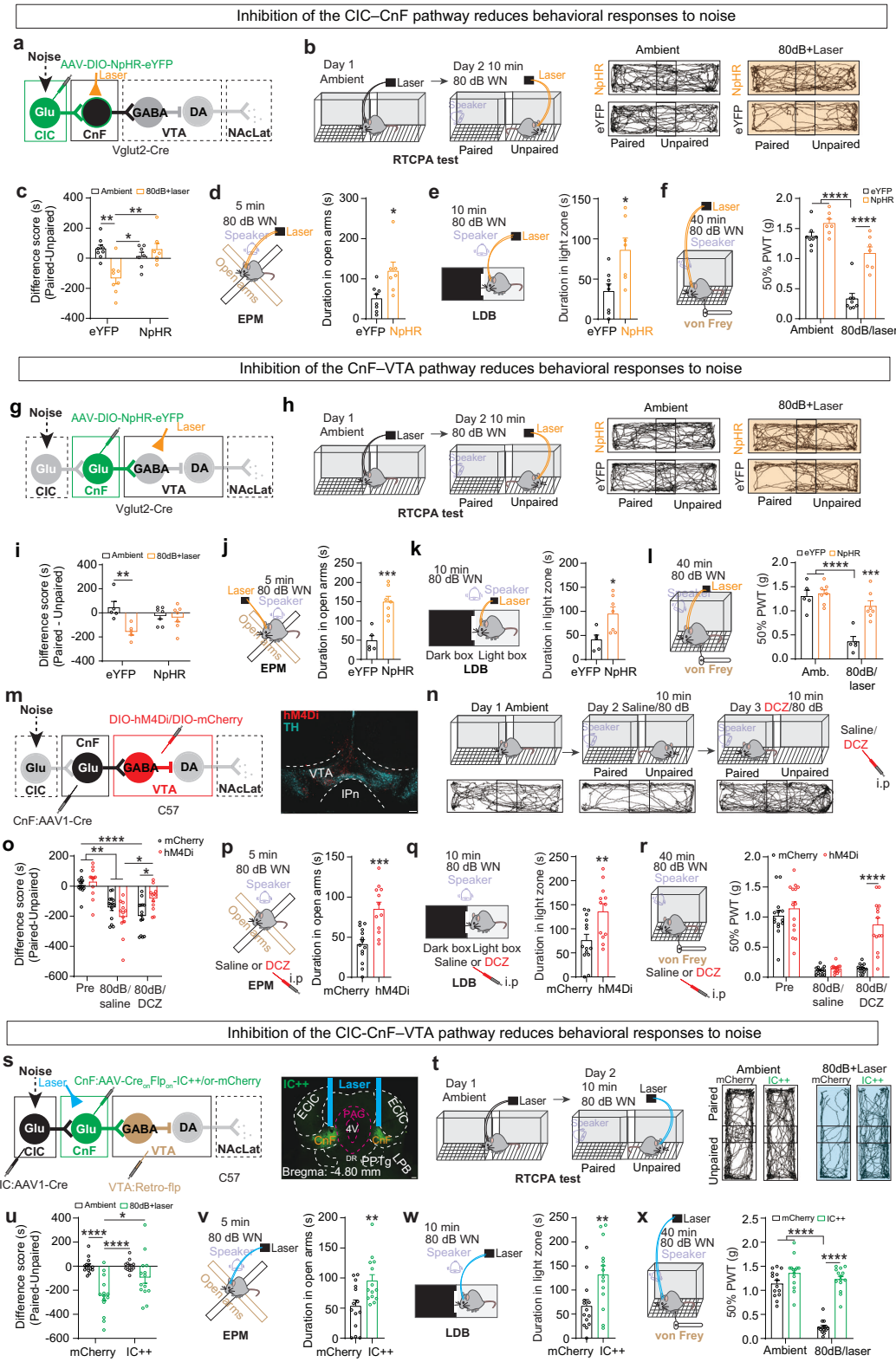

vNAcMed in response to 80 dB noise instead of inhibition (Figs. 6e, f; and Supplementary Fig. 7l). Although DA in the vNAcMed does not seem to respond to noise as significantly as DA in the NAcLat, the variability in the data and the limited statistical power may also affect the experimental results. Therefore, we cannot completely rule out the possibility that DA in the vNAcMed is involved in the processing and response to noise information. These results support the notion that mesoaccumbal DA pathways exhibit high heterogeneity[44,45]. In addition, we injected a Cre-dependent Ca^{2+} indicator, GCaMP6m, into the VTA of DAT-Cre mice and implanted an optical fiber into the NAcLat (Supplementary Fig. 7m, n). This allows us to confirm that 60 dB and 80 dB white noise reliably decrease Ca^{2+} signals in NAcLat DA terminals

Fig. 5 | Silencing of the CIC → CnF → VTA circuit prevents loud sound-induced negative emotional responses. a Experimental design. **b** Experimental design and representative traces of eYFP- and NpHR-expressing mice in the RTCPA test. **c** Difference score (eYFP: 8 mice; NpHR: 7 mice, Two-way ANOVA with Tukey's post hoc test). **d** Time spent in the open arms (eYFP: 8 mice; NpHR: 7 mice, Unpaired t-test). **e** Time spent in the light-box (eYFP: 8 mice; NpHR: 7 mice, Unpaired t-test). **f** 50% PWT tests (eYFP: 8 mice; NpHR: 7 mice, Two-way ANOVA with HolmSidak's post hoc test). **g**–**l** same as above **a**–**f** but for silencing of CnF^{glu} → VTA circuit (eYFP: 5 mice; NpHR: 7 mice). **m** Experimental design (left). (Right) IHC staining showing hM4Di-expressing (red) cells in the VTA are TH -immunonegative (cyan). Scale bar, 100 μm. **n** Experimental design (top) and (bottom) trajectories of hM4Di-expressing mouse in the CPA chamber. **o** Difference score (mCherry: 14 mice; hM4Di: 12 mice, Two-way ANOVA with Tukey's post hoc test). **p** Time spent in the open arms in mCherry-(black) and hM4Di-expressing (red) mice after receiving 100 μg/kg DCZ injection (mCherry: 14 mice; hM4Di: 12 mice, Unpaired t-test). **q** Time spent in the light-box in mCherry- (black) and hM4Di-expressing (red) mice after receiving 100 μg/kg DCZ injection. (mCherry: 14 mice; hM4Di: 12 mice, Unpaired t-test). **r** 50% PWT tests (mCherry: 14 mice; hM4Di: 14 mice, Two-way ANOVA with HolmSidak's post hoc test). **s** Experimental design (left). Coronal brain slice image showing IC + + expression (green) in the CnF (right). **t** Experimental design and representative traces of mCherry- and IC + +-expressing mice in the RTCPA test. **u** Difference score ($n = 14$ mice, Two-way ANOVA with Holm-Sidak's post hoc test). **v** Time spent in the open arms ($n = 14$ mice, Unpaired t-test). **w** Time spent in the light-box ($n = 14$ mice, Unpaired t-test). **x** 50% PWT tests ($n = 14$ mice, Two-way ANOVA with HolmSidak's post hoc test). All graphs are represented as mean ± SEM. $^{*}p < 0.05$, $^{**}p < 0.01$, $^{***}p < 0.001$ or $^{****}p < 0.0001$.

(Supplementary Fig. 7o, p). However, compared with the DA sensor (dLight) recordings, we observed a biphasic suppression of NAcLat DA terminals, indicating the possible involvement of additional parallel pathways in noise-induced NAc DA release[46].

To further verify the causal relationship between reduced DA activity in NAcLat and negative emotional responses induced by loud noise, we infused SKF81297, a selective D1 receptor agonist, into the NAcLat (Fig. 6i) or optogenetically activated dopaminergic terminals in the NAcLat (Fig. 6p). Both manipulations successfully prevented loud noise-induced aversion, anxiety, and pain (Figs. 6i–w). However, we found that infusing SKF81297 into the NAcMed did not affect noise-induced aversive behaviors (Supplementary Fig. 7q–v). This further confirms that, compared to the NAcMed DA, the NAcLat DA plays a more important role in the regulation of noise-induced negative emotions. Consistent with previous studies[38], optogenetic stimulation of dopaminergic terminals in the NAcLat elicited a reward response (Supplementary Fig. 8a–c). However, direct excitation of the NAcLat DA pathway did not produce anxiolytic effects in the EPM and LDB tests (Supplementary Fig. 8d–e). Given the potential ceiling effect in normal mice in the EPM and LDB tests, we cannot completely rule out the possibility that direct activation of this pathway may only enhance reward behavior without affecting anxiety levels. This suggests that while exciting NAcLat DA activity can prevent loud noise-induced aversion and anxiety, these effects might be mediated, at least in part, through reward-related mechanisms. Furthermore, excitation of the VTA^{DA}→NAcLat rewarding pathway[38,39] is critical for counteracting generalized negative emotions induced by loud noise (Fig. 6x).

Collectively, our results highlight a crucial role for the CIC^{glu}→CnF^{glu} → VTA^{GABA} → $lVTA^{DA}$ circuit in coding negative emotions induced by aversive sounds. Our data suggest a model where CIC^{glu} neuronal activity serves as a key node, determining whether aversive sound information is relayed to the lVTA DA system via the CnF^{glu} → VTA^{GABA} circuit (Fig. 7).

Discussion

While emotions are generally believed to emerge from the interaction between bottom-up and top-down processes, the mechanisms by which emotions arise from low-level processes that provide rapid, bottom-up affective evaluations of stimuli remain largely unexplored. In this study, we demonstrate that the CIC^{glu}→CnF^{glu} → VTA^{GABA} circuit, a noncanonical auditory pathway, governs the perception of noise-induced negative emotions. Our results underscore the role of bottom-up response systems in encoding both the perceptual and affective properties of stimuli[47]. Moreover, since the CIC^{glu}→CnF^{glu} → VTA^{GABA} circuit responds to other aversive stimuli besides noise, this circuit we identified may be a potential generalist target for anxiety treatments.

CIC^{glu} neurons integrate multiple sensory stimuli

Consistent with the established view that the CIC is predominantly considered an auditory structure[19,20], we found that CIC^{glu} neurons responded to various intensities of white noise in a dose-dependent manner. Surprisingly, this same population of CIC^{glu} neurons also responded to other aversive sensory stimuli. Rabies-mediated retrograde tracing revealed that CIC^{glu} neurons primarily receive inputs from auditory-related brain regions, but we also observed rabies-labeled cells in aversion-related brain areas, such as the LPB and PAG (Supplementary Fig. 2), providing an explanation for the responsiveness of CIC^{glu} neurons to nociceptive stimuli (Fig. 2 and Supplementary Fig. 1). In line with these observations (Supplementary Figs. 1, 2), we found that excitation of CIC neurons modulated motivated behaviors (Supplementary Fig. 3). Collectively, these data suggest that the CIC functions as a node integrating various sensorimotor modalities in a highly interconnected manner, complementing its well-established role in auditory perception.

CnF relays negative stimuli from CIC to VTA^{GABA} neurons

Although we found that CIC-targeted MG neurons did not differentiate between different intensity levels of white noise and that optogenetic stimulation of this pathway did not induce aversion, we cannot entirely exclude the possibility that the MG might influence the mesolimbic DA system and modulate motivated behaviors through other parallel circuits[48]. For example, the MG might relay CIC-encoded aversive information to VTA^{GABA} neurons to encode negative valence. However, our mapping of MG neuronal projections in the midbrain showed substantial projections to the red nucleus but not in the VTA (Supplementary Fig. 7). This suggests that the MG does not directly relay CIC's aversive information to VTA^{GABA} neurons. Additionally, we observed that inhibition of the auditory cortex had minimal effects on preventing acute noise-inducing negative emotions and NAcLat DA inhibition. Thus, the CIC^{glu} → MG pathway may primarily relay salient stimuli to the cortex. However, we can't exclude that top-down control might regulate emotional responses and dopamine release in other brain regions through parallel circuits[49]. In contrast, CIC-targeted CnF neurons and their downstream VTA^{GABA} neurons required activation by noise levels exceeding 50 dB and by painful stimuli. Inhibition of the CIC^{glu}→CnF^{glu} → VTA^{GABA} circuit effectively blocked the generalization of noise-induced negative emotions, further supporting the critical role of CnF neurons in processing aversive stimuli[29,50]. Together, our results suggest that CIC^{glu} neurons likely integrate acoustic stimuli and relay sounds of varying intensities to downstream nuclei to encode salience or valence[11,22,37].

Moreover, both CIC-targeted MG neurons and CIC-targeted CnF neurons responded to both nociceptive and acoustic stimuli, suggesting that multiple sensory modalities converge within a shared information pathway to integrate and relay information to common downstream targets, encoding salience or valence and instructing subsequent behavioral responses. However, it remains elusive how CIC^{glu} neurons filter and integrate sound stimuli with varying degrees of negative valence to modulate the VTA DA system via the CnF^{glu}-VTA^{GABA} circuit. One possibility is that CIC^{glu} activity is influenced by the

https://doi.org/10.1038/s41467-025-59956-z

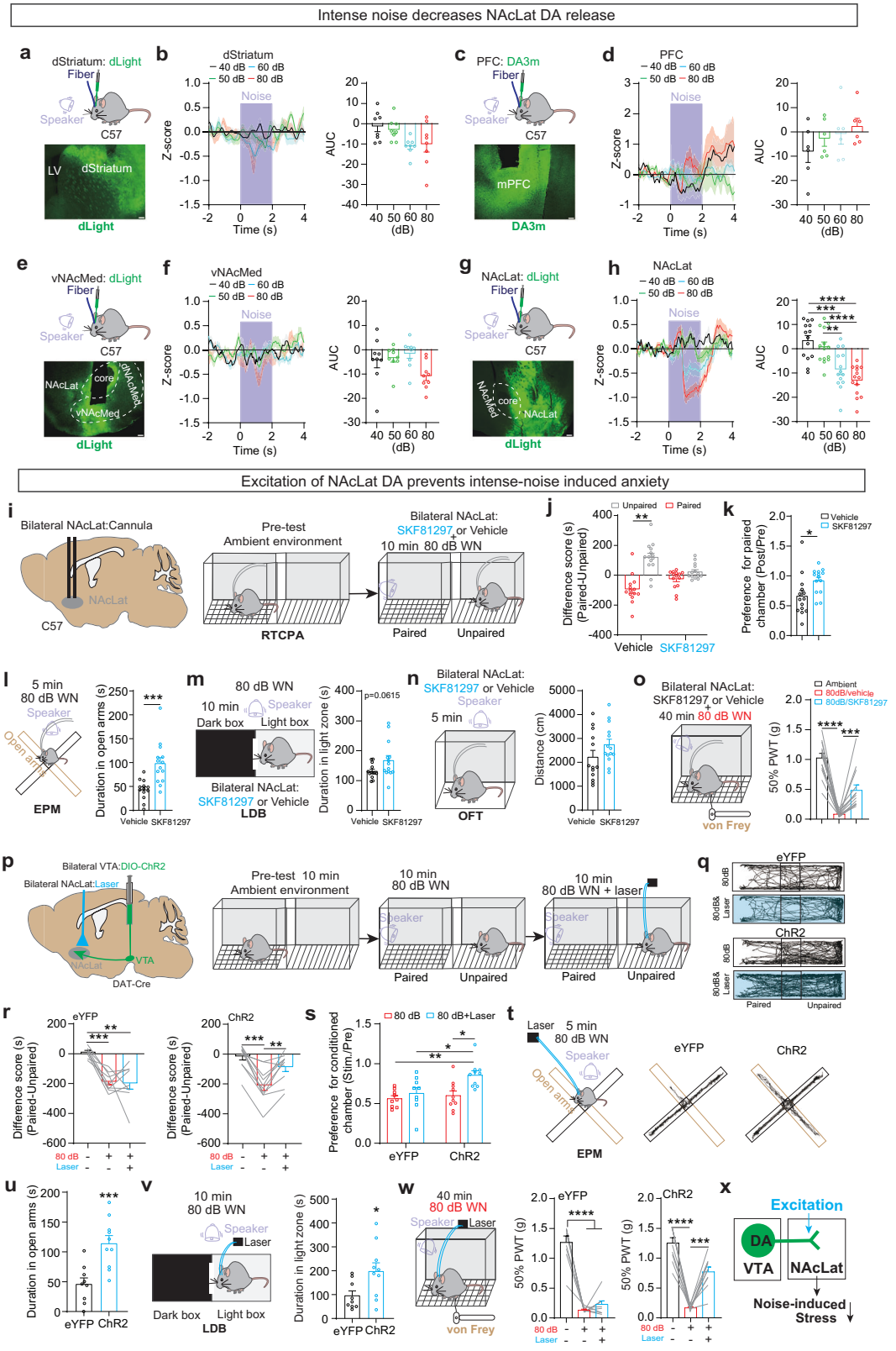

characteristics of sound stimuli, including their intensity and spectrotemporal features[14–16].

Noise affects emotions via dopamine

A recent study identified a corticothalamic top-down circuit that mediates sound-induced analgesia[49], with this phenomenon potentially being indirectly linked to the VTA DA system[51,52]. However, it remains unclear whether sound-induced analgesia is a common occurrence across different species[53]. In our study, we identified a noncanonical auditory circuit that overlaps with a nociceptive circuit in encoding negative emotions through the inhibition of NAcLat DA activity. Selective activation of NAcLat DA activity effectively prevented noise-induced negative emotions, likely by enhancing reward and positive mood. In addition, we observed that acute

Fig. 6 | Excitation of NAcLat DA alleviates Noise-induced negative emotional responses. a Recording DA release in the dorsal striatum (dStriatum, bottom; scale bar, 100 μm), dLight (green). **b** Z-score average (left). (Right) AUC during sound stimulation ($n = 8$ mice, one-way ANOVA with Tukey's post hoc test). (**c**–**h**) Same as the (**a**, **b**), but for the prefrontal cortex (PFC, **c**, **d** $n = 6$ mice, one-way ANOVA with Tukey's post hoc test), the ventral NAc medial shell (vNAcMed, **e**, **f**; $n = 9$ mice, one-way ANOVA with nonparametric test), and the NAcLat (**g**, **h**; $n = 14$ mice, one-way ANOVA with Tukey's post hoc test). **i** Experimental design. **j** Difference score ($n = 14$ mice, Paired t-test). **k** Preference score ($n = 14$ mice, Unpaired t-test). **l** Time spent in the open arms in mice infused with vehicle ($n = 13$ mice) or SKF81297 ($n = 14$ mice), Unpaired t-test. **m** Time spent in the light box in mice infused with vehicle ($n = 13$ mice) or SKF81297 ($n = 14$ mice), Unpaired t-test. **n** Average travel distance. Vehicle: 13 mice; SKF81297: 14 mice, Unpaired t-test. **o** Average 50% PWT. ($n = 14$ mice, one-way ANOVA with Tukey's post hoc test). **p** Experimental design. **q** Representative trajectories of eYFP-expressing mice (top) and ChR2-expressing mice (bottom) in the RTCPA test. **r** Difference score (eYFP: 9 mice, ChR2: 10 mice, one-way ANOVA with Tukey's post hoc test). **s** Preference score (eYFP: 9 mice, ChR2: 10 mice, Two-way ANOVA with Holm-Sidak's post hoc test). **t** Schematic of EPM test with optogenetic activation (left) and representative mouse traces of eYFP-expressing (middle), and ChR2-expressing mouse (right). **u** Time spent in the open arms (eYFP: 9 mice, ChR2:10 mice, Unpaired t-test). **v** Schematic of LDB test with optogenetic activation (left) and (right) time spent in the light-box (eYFP: 9 mice, ChR2:10 mice, Unpaired t-test). **w** 50% PWT test for mice experienced 40 min 80 dB noise and light stimulation. (eYFP: 9 mice, ChR2: 10 mice, one-way ANOVA with Turkey post hoc test). **x** Schematic of the experimental model. All graphs are represented as mean ± SEM. $^{*}p < 0.05$, $^{**}p < 0.01$, $^{***}p < 0.001$ or $^{****}p < 0.0001$.

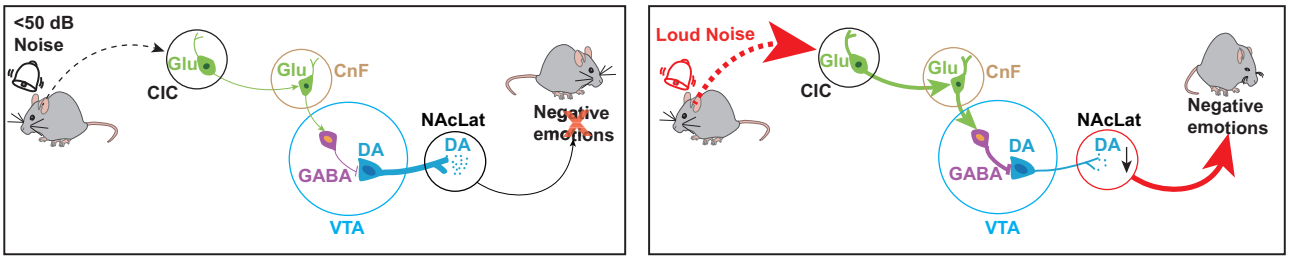

Fig. 7 | Work model. Schematic illustrating a neural circuit mechanism for distinguishing neural and aversive sound information. Left panel, the CIC^{glu} neurons respond to < 50 dB sounds. The activity of these neurons fails to recruit VTA^{GABA} neurons to inhibit the NAcLat-projecting VTA^{DA} neurons. As a result, the animals maintain a low negative emotional state. Right panel, the activity of the CIC^{glu} neurons is dramatically activated by loud sounds. These neurons convey the aversive sound information to CnF^{glu} neurons to drive VTA^{GABA} neurons and encode negative valence by inhibiting the NAcLat-projecting VTA^{DA} neurons. As a result, the animals exhibit a negative emotional state.

loud noise consistently decreased NAcLat DA activity, and promoted aversion and anxiety, though it did not affect pain perception. Interestingly, excitation of NAcLat DA alleviated chronic noise-induced mechanical pain, suggesting that noise-induced pain is at least partially attributable to NAcLat DA inhibition. Acute loud noise stimulation may place animals in a high-stress state, influencing pain behavior[54], while chronic noise might affect the mesolimbic DA system through other parallel pathways[46,55]. However, we cannot rule out the possibility that other brain regions may play a more significant role in chronic noise-induced pain, and we will investigate this in future experiments.

It appears that both negative valence sounds ("unpleasant" sounds) and positive valence sounds ("pleasant" sounds) might regulate the DA system through distinct, yet currently unknown, neural circuits. Future studies should explore how the auditory system conveys information about positive valence sounds to the midbrain DA system.

Local VTA inhibitory circuits in negative emotions

In local DA circuits, VTA^{GABA} neurons provide a major source of inhibitory control and play a crucial role in promoting aversion by inhibiting VTA DA neurons[31,32,39,56]. However, VTA^{GABA} neurons are not a homogeneous population[57]. In addition to their local inhibitory role, some VTA^{GABA} neurons project to various brain regions[33], influencing behavioral outcomes. While the involvement of other parallel circuits in sound-induced negative emotions through the VTA DA system cannot be excluded, these studies support the hypothesis that distinct inhibitory subpopulations of VTA^{DA} neurons are specifically involved in different behaviors[33]. Furthermore, VTA glutamate neurons are also important in aversion-based behaviors[58,59]. We observed that the majority of CnF-targeted VTA neurons were GAD67-positive (~64%) but not TH-positive (Fig. 3), suggesting that the CnF may form synaptic connections with VTA glutamate neurons. We propose that unpleasant sounds might induce aversion by activating VTA glutamate neurons via the CIC^{glu}-CnF^{glu} pathway or other parallel pathways[57], which warrants further investigation in future studies.

In summary, this study identified and characterized a non-canonical $CIC^{glu} \rightarrow CnF^{glu} \rightarrow VTA^{GABA}$ auditory circuit involved in processing aversive sounds. We demonstrate that activation of this circuit by aversive sounds leads to the inhibition of dopamine release in the NAcLat, thereby regulating negative emotions through the activation of VTA^{GABA} neurons. The identification of this indirect inhibitory circuit not only provides a mechanistic understanding of how sensory information is integrated by the mesolimbic dopamine system but also suggests potential therapeutic approaches for alleviating negative emotions induced by aversive sensory stimuli.

Methods

Subjects

8-12 weeks C57BL/6J, Vglut2-ires-Cre (Jackson Laboratory, strain name *B6J;129S6-(FVB)-Slc17a6$^{tm2(cre)Lowl}$/MwarJ*, stock number 028863), Vgat-ires-Cre (Jackson Laboratory, strain name *Slc32a1$^{tm2(cre)Lowl}$/J*, stock number 016962), DAT-ires-Cre (Jackson Laboratory, strain name *B6J.SHJ-Slc6a3$^{tm1(cre)Bkmn}$/J*, stock number 006660), and Ai14 Cre reporter line (Jackson Laboratory, strain name *B6;129S6 Gt(ROSA) 26Sor$^{tm14(CAG-tdTomato)Hze/J}$*, stock number 007908) mice were used. Mice were maintained on a 12:12-h light cycle (lights on at 07:00) with water and food ad libitum and room temperature of 22–25 °C and 55% humidity. Male and female mice were used in our experiments. All animal experiments were conducted by the guidance for the care and use of laboratory animals of Zhejiang University.

Stereotaxic surgeries

Viral vectors. AAV5-EF1α-DIO-hChR2(H134R)-eYFP, AAV5-CAG-Flex-GCaMP6m-WPRE-SV40, pENN.AAV1.hSyn.Cre.WPRE.hGH (AAV anterograde), AAV5-EF1a-DIO-eNpHR3.0-eYFP, pAAV-flex-taCasp3-TEVp, $AAV_{(2/8)}$-hSyn-DIO-hM4D(Gi)-mCherry, AAV5-hSyn-hChR2(H134R)-mCherry, AAV5-hSyn-eYFP, AAV8-nEF-C_{on}/F_{on}-IC + +-eYFP, AAV8-nEF-

C_{on}/F_{on}-mCherry, and AAV5-CAG-dLight1.3b were prepared by the Addgene. AAV5-EF1α-DIO-eYFP, AAV5-EF1α-DIO-mCherry, AAV2-retro-hSyn.cre.WPRE.pA, and AAV2-retro-hSyn.Flpo.WPRE.pA were prepared by the Shanghai Taitool Bioscience. The final titer was estimated to be ~10^{12} genome copies per milliliter. RetroAAV11-hSyn-DIO-eYFP, RetroAAV11-hSyn-DIO-mCherry, AAV8-hEF1α-DIO-synaptophysin-mCherry (~10^{12}), AAV8-CAG-DIO-TVA-mCherry(~10^{12}), AAV8-CAG-DIO-rabies glycoprotein G (~10^{12}), and EnvA-G deleted rabies-eGFP (~10^{8}) were prepared by BrainCase (China). AAV9-hSyn-DA3m-WPRE-hGH (~10^{12}) was prepared by BrainVTA (China).

Viral injections. Mice were anesthetized with pentobarbital sodium (100 mg/kg, intraperitoneal), and stereotaxic surgeries were performed using a stereotaxic instrument (RWD life science). 100-300 nL of concentrated AAV virus solution was injected into the CIC (150 nL; bregma: −5.2 mm; lateral: 1.0 mm; ventral: −2.1 mm), CnF (80 nL; bregma: −4.84 mm; lateral: 1.25 mm; ventral: −2.75 mm), MG (200 nL; bregma: −3.28 mm; lateral: 1.8 mm; ventral: −3.0 mm), nucleus accumbens lateral shell (NAcLat, 250 nL, bregma: 0.98 mm, lateral: 2.00 mm, ventral: −4.80 mm), prefrontal cortex (PFC, 100 nL; bregma: 1.54 mm; lateral: 0.30 mm; ventral: −2.75 mm), ventral NAc medial shell (vNAcMed, 250 nL; bregma: 0.98 mm; lateral: 0.50 mm; ventral: −5.18 mm), dorsal striatum (250 nL; bregma: 1.00 mm; lateral: 1.80 mm; ventral: −2.65 mm), or VTA (300 nL; bregma: −3.4 mm; lateral: 0.4 mm; ventral: −4.3 mm) using a syringe pump (Ditron-tech LSP02-3B) at 100 nL/min. Injection sites were confirmed in all animals by preparing coronal sections (100 μm) after behavioral tests.

Retrograde or anterograde tracing. C57BL/6 J or Ai14 mice were injected unilaterally with Retro-beads (100 nL), pENN.AAV1.hSyn.-Cre.WPRE.hGH (anterograde AAV1-Cre), AAV2-retro-hSyn.cre.WPRE.pA (RetroAAV2-Cre), RetroAAV11-hSyn-DIO-eYFP or RetroAAV11-hSyn-DIO-mCherry into the CIC (150 nL; bregma: −5.2 mm; lateral: 1.0 mm; ventral: −2.1 mm), CnF (80 nL; bregma: −4.84 mm; lateral: 1.25 mm; ventral: −2.75 mm); MG (150 nL; bregma: −3.28 mm; lateral: 1.8 mm; ventral: −3.0 mm), or/and VTA (150 nL; bregma: −3.4 mm; lateral: 0.4 mm; ventral: −4.3 mm). The detail of injections was noted in each figure. To ensure the AAV1-Cre virus is injected into the right site, a control viral (AAV-hSyn-eYFP or mCherry) is mixed in the AAV1-Cre for the identification of the viral injection site. 10 days after injection, mice were perfused with 4% PFA in PBS and coronal brain sections (100 μm) were collected for imaging experiment (Olympus confocal microscope FV1200). In the experiment of double-labeling CIC^{glu} neurons that project to MG and CnF, the RetroAAV11-hSyn-DIO-eYFP and RetroAAV11-hSyn-DIO-mCherry were alternately injected into the MG and CnF of Vglut2-Cre mice. The retroAAV11-eYFP and retro-AAV11-mCherry labeled cells in the CIC were manually counted using ImageJ.

Rabies tracing. The Cre-dependent helper viruses (AAV-CAG-DIO-TVA-mCherry and AAV-CAG-DIO-RVG, 1:1 mixed; ~10^{12}) were injected into the CIC (bregma: −5.2 mm; lateral: 1.0 mm; ventral: −2.1 mm) of Vglut2-Cre mice. 3 weeks later, a genetically modified rabies virus (RV)-eGFP pseudotyped with the avian envelope protein was delivered to the same coordinates after the injection of helper viruses. 7 days after RV injection, mice were perfused with 4% PFA in PBS. 100 μm coronal brain sections were collected for imaging. All brain sections were imaged using an Olympus slide scanner microscope (VS120). Whole-brain counting of RV-labeled cells was done manually using Image J.

In vivo optogenetic experiments. Experiments were performed 4-5 weeks after stereotactic surgery. AAV-ChR2, -eYFP,-taCasp3, or -NpHR injected mice received unilateral or bilateral implantation of chronically implanted optical fiber(s) (200 μm, NA = 0.37; Inper Inc.) dorsal to the CIC (bregma: −5.2 mm; lateral: 1.0 mm; ventral: −1.8 mm), MG (bregma: −3.2 mm; lateral: 1.8 mm; ventral: −2.7 mm), VTA (bregma: −3.4 mm; lateral: 0.5 mm; ventral: −4.1 mm), NAcLat (bregma: 0.98 mm, lateral: 2.00 mm, ventral: −4.30 mm), CnF (bregma: −4.84 mm; lateral: 1.25 mm; ventral: −2.55 mm), and fixed optical fiber to the skull with small screws and dental cement (Henan Reding Dental Material Co.). Mice were allowed to recover for ~7 days at least after surgery. For behavioral tests, we used 20 Hz-5 ms, ~2 mW/mm^2 473 nm light to unilaterally stimulate CIC, CnF, VTA, PAG, or MG, or to bilaterally stimulate NAcLat; Bilaterally applied continuous 589 nm light for (CIC^{glu} cell bodies, CIC^{glu} terminals in CnF, CnF^{glu} terminals in VTA) NpHR inhibition (~5 mW/mm^2). Viral expressions and optical fiber implanted sites were confirmed in all animals by preparing coronal sections (100 μm). Although optical fiber placements varied slightly from mouse to mouse, behavioral data from all mice were included in the study.

Cannula implantation. A dual-cannula with a diameter of 200 μm (RWD Life Science) was bilaterally implanted into NAcLat (bregma: 1.10 mm, lateral: ±1.75 mm, ventral: −4.30 mm) or NAcMed (bregma: 1.18 mm, lateral: ±0.50 mm, ventral: −4.50 mm). To prevent the cannula from clogging during the next 10 days recovery period, two dummy cannulas (diameter ~100 μm; RWD Life Science) with a cap were inserted into the cannulas.

In vivo fiber photometry experiments. Calcium transients were measured using commercial fiber photometry equipment (Inper Inc.; RWD life science) same as we used in the previous study[42]. Briefly, 2 weeks after GCaMP6m-, DA3m- or dLight1.3-AAVs injection, the mice received unilateral implantation of a chronically-implanted optical fiber (400 μm, NA = 0.48; Inper Inc.) into the CIC (bregma: −5.2 mm; lateral: 1.0 mm; ventral: −2.0 mm), CnF (bregma: −4.84 mm; lateral: 1.25 mm; ventral: −2.5 mm), VTA (bregma: −3.4 mm; lateral: 0.5 mm; ventral: −4.2 mm), MG (bregma: −3.2 mm; lateral: 1.8 mm; ventral: −2.7 mm), PFC (bregma: 1.54 mm; lateral: 0.30 mm; ventral: −2.50 mm), vNAcMed (bregma: 0.98 mm; lateral: 0.50 mm; ventral: −5.00 mm), dorsal striatum (bregma: 1.00 mm; lateral: 1.80 mm; ventral: −2.45 mm), or NAcLat (bregma: 0.98 mm, lateral: 2.00 mm, ventral: −4.50 mm). Recordings were performed at 4 weeks after viral injections. Fluorescence signals were obtained by stimulating cells expressing GCaMP6m, DA3m, or dLight1.3 with a 473 nm LED (20 μW), while calcium-independent signals were obtained by stimulating these cells with a 405 nm LED (20 μW). 473 nm and 405 nm LED light were alternated at 20 or 30 Hz and light emission was recorded using a sCMOS Camera (Photometrics Prime).

For recordings of glutamatergic or GABAergic neurons in CIC, CIC-targeted neurons in CnF or MG, GABAergic neurons in VTA, or dopaminergic activity in NAcLat to different stimuli: (1) Sounds: mice received 10-15 trails of different intensities of white noise (from 40-90 dB) through a closely positioned audio speaker (Momoho). The sound pressure level was measured by a digital sound level meter GM1351 (Shenzhen Jumaoyuan Science and Tech Co., Ltd). (2) Tail pinch and back brush: mice received 10–20 tail pinches (~3 cm from tip of tail) using forceps or brushed mouse's back using a brush (10 s duration, 30 s intervals between stimuli). (3) Tail shock: electrode pads were placed on the tail (the distance of positive and negative pads is ~1 cm) and mice received 10-20 trials of 0.1 mA or 0.5 mA tail shocks (2 s duration, 28 s intervals between shocks). (4) Hot or cold water: the ~3 cm tip of the mouse's tail was placed in a temperature-controlled water bath ranging from 0 °C to 55 °C, 10 s duration, 10-15 trials, and 60 s intervals between each temperature level. Hot or cold water, back brush, and tail pinch were manually applied to mice, and experimental time stamps were acquired using a manual TTL pulse generator. Time stamps of sounds and tail shocks were automatically generated by a pulse generator (Inper Co., Ltd). All stimuli were synchronized to calcium recordings by applying the stimulus at the designated time during the recording.

Given that some CIC neurons respond to locomotion, to confirm the elevated of CIC^{glu} Ca^{2+} signals were from aversive stimuli, but not barely from movement, we repeated the white noise (2 s duration, 15 s intervals), and shock (2 s duration, 15 s intervals) stimuli experiment after mice were sedated with choral hydrate (5%, i.p.). We chose chloral hydrate because of its strong sedative effects but does not block nociceptive information processing. High concentrations of chloral hydrate (20%) are highly irritating and may cause intestinal obstruction, peritonitis, and gastric ulcers in rats. So, to reduce the side effect we chose 5% chloral hydrate to sedate mice (0.15 ml per mouse, mouse's body weight about 24-26 g). After the Ca^{2+} recording experiment, mice were immediately anesthetized using pentobarbital sodium (200 mg/kg) and perfused with 4% PFA in PBS for the histological experiment.

For fiber photometry recordings of dopamine release in the NAcLat or calcium fluorescence of GABAergic neurons or dopamine neurons in VTA when optogenetic excitation of CIC^{glu} neurons or CIC^{glu} projections in CnF, given that CIC neurons do not directly project to VTA and NAcLat, we can exclude overlapping between ChR2-eYFP and GCaMP or dLight signals, and as well as through light intensities: GCaMP or dLight excitation was performed using LED light intensities at 20 μW/mm^2 and ~2 mW/mm^2 light was used for ChR2 excitation. Experimental time stamps were acquired using TTL pulses generated by a pulse generator (Inper Co., Ltd). The Z-Score or AUC interval was defined as the entire laser stimulation period (0-2 sec).

Regarding quantification, the filtered 405 nm signal was aligned with the 470 nm signal by using the least-square linear fit. The fitted 405 nm signal was then subtracted from the 470 nm signal to obtain the movement and bleaching-corrected signal. dF/F was calculated according to (470 nm signal-fitted 405 nm signal)/(fitted 405 nm signal). And the standard z-score calculation method is used, that is, Z-score = (x-mean)/std, x = dF/F. Baseline normalization was performed on the original dF/F signal using the time window −2 to 0 sec. Thus, Z-score reflects the number of standard deviations from the mean and it is possible that the baseline is not at 0. To exclude the influence of motion on in vivo calcium imaging, all fiber photometry experiments were performed in head-fixed moving mice. However, the whole-body restraint can cause stress in animals, affecting experimental results. We adopt a turntable type of head-fixed device to perform the calcium imaging on mice. This device allows animals to freely walk or run but the animal's head position remains stable. This approach ensures that the animal maintains a stable position during the recording, which allows experimenters to easily administrate different manual stimuli to the animal, and mark the time stamps of the stimuli[23].

For fiber photometry recordings of DA release in the NAcLat, calcium fluorescence of GABAergic neurons in the VTA, and calcium fluorescence of glutamatergic neurons in the CIC under long-term 80 dB noise stimulation (Fig. R1), injection of AAV-Flex-GCaMP to the CIC or VTA of Vglut-Cre or Vgat-Cre mice, respectively. These mice also received a Dlight injection into the NAcLat to monitor DA release. After placing the mice in the test box for a 5-minute environmental adaptation, we exposed them to 5 minutes of 80 dB noise stimulation. We continued monitoring calcium activity in the three brain regions for another 5 minutes after the noise off. The filtered 405 nm signal was aligned with the 470 nm signal by using the least-square linear fit. The fitted 405 nm signal was then subtracted from the 470 nm signal to obtain the movement and bleaching-corrected signal. dF/F was calculated according to (470 nm signal-fitted 405 nm signal)/(fitted 405 nm signal). We calculated the AUC changes in calcium activity in these regions before and after the noise stimulation. Note that due to surgery and virus expression, calcium signals from these regions weren't always recordable in all mice. Thus, the n numbers for each group are different.

In vivo microendoscopic (miniscope) calcium imaging. To optically record from CIC^{glu} neurons by using miniscope calcium imaging, 200 nL $AAV_{(2/5)}$-CAG-Flex-GCaMP6m was injected into the CIC (bregma: −5.2 mm; lateral: 1.0 mm; ventral: −2.0 mm) of Vglut2-Cre mice. After two weeks of viral expression, a 500 μm diameter-5 mm length gradient-index (GRIN) lens (Shenzhen Anshen Bio-Tech Co.) was slowly (50 μm/min) implanted into the CIC (bregma: −5.2 mm; lateral: 1.0 mm; ventral: −2.0 mm) and a matching baseplate (Shenzhen Anshen Bio-Tech Co.) was positioned over the GRIN lens and cemented with dental acrylic. After two weeks of GRIN lens implantation, calcium fluorescence videos were recorded through a customized miniature microscope (GLOBAL BIOTECH INC.; Inper Co., Ltd) at 20 Hz using the open-source data acquisition software developed by Aharoni-Lab (https://github.com/Aharoni-Lab/Miniscope-DAQ-QT-Software). Raw videos from each imaging session used the motion correction function of NoRMCorre[60] in MATLAB(2021b) to correct motion-induced artifacts across frames. To normalize image frames prior to cell sorting, (F-F0)/F0 (dF/F) was applied to each frame, where F0 was the de-trended mean frame. dF/F normalized videos were de-noised using an FFT spatial band-pass filter in ImageJ. Next, we implemented a constrained nonnegative matrix factorization algorithm to extract neuronal signals (https://github.com/zhoupc/CNMF_E/). The automated recognized neurons were visually inspected, and those displaying nonneuronal morphology were removed. Each neuron was defined as excited or inhibited cells in 80 dB white noise (2 s), 0.5 mA electric shock (1 s), tail pinch (1 s), or 55 °C hot water (10 s) stimulation (10 trials) as compared to the dF/F of stimulation (5 s) and of the equivalent baseline period (5 s) using a Wilcoxon signed-rank test with a significance threshold of $p < 0.05$. To reliably track responses of the same neuron experiencing all those stimuli, we performed all those stimuli in one recording session, and then determined the same cell based on its location and morphology information. To exclude the influence of motion on in vivo calcium imaging, the experiment was performed in head-fixed moving mice.

In vivo Electrophysiology Recording[26]. AAV2/5-DIO-ChR2 virus was injected into the CIC of Vglut2-Cre mice (bregma: −5.2 mm; lateral: 1.0 mm; ventral: −2.0 mm). 3 weeks later, mice were implanted with a custom-built drivable optrode into the dorsal CIC (bregma: −5.2 mm; lateral: 1.0 mm; ventral: −1.1 mm), which consisted of sixteen microwires (12 μm diameter; Stablohm 675; California Fine Wire, Grover Beach, CA) glued to a 100 μm optical fiber using hydrogel. The tetrodes protruded from the tip of the optical fiber by ~0.2 mm. Wire tips were cut flat and gold plated to reduce impedance to ~200 kΩ at 1 kHz. A small screw was fixed to the skull and served as a ground electrode. After tetrode implantation, animals were allowed to recover for ~10 days. Neural signals were recorded using a Digital Apollo II system (Bio-Signal Technologies: Nanjing, China) with a head stage pre-amplifier (Bio-Signal Technologies: Nanjing, China). Recorded signals were filtered using high-pass filter at 300 Hz and digitized at 30 kHz. At the end of each recording session, the optrode was ventrally moved for ~40μm. The final recording location was verified using histology after the electrolytic lesion.

Spikes were sorted based on the waveform energy and the first three principal components of the spike waveform on each stereotrode channel. Spikes were sorted offline using Offline Sorter V2.8.5 software (Plexon) and data was analyzed using NeuroExplorer V5.403 (Plexon).

ChR2-tagged neurons were identified by delivering 473 nm (~0.4 mW/mm^2, 3-ms pulses) of light at 1-Hz frequency for 5 min. A unit was identified as ChR2 expressing if spikes were evoked by laser pulses reliably with short first-spike latency, and with the waveforms of light-evoked and spontaneous spikes highly similar.

After ChR2-tagged neurons were identified, various aversive stimuli (80 dB white noise, tail pinch, and 55 °C hot water) were sequentially applied to mice. For noise stimulation, 80 dB white noise was applied to the mice through a closely positioned audio speaker (5 s duration, 30 s intervals, 10–15 trials). For painful stimulation, mice received tail pinches using forceps (3–4 cm away from tip of the tail, 5 s duration, 30 s intervals, 10–15 trials). For the heat stimulus, the tip of the tail was placed in a temperature-controlled water bath (55 °C, 5 s duration, 60 s intervals, 7–10 trials). The experimental time stamps were acquired using a manual TTL pulse generator. To determine whether aversive stimuli altered CIC^{glu} neural activity patterns, the 5 s baseline mean firing rate before the aversive stimulus was compared to the mean firing rate during the aversive stimuli using paired t-tests ($P < 0.05$ for excited or inhibited; $P > 0.05$ for non-response). To exclude the influence of motion on in vivo electrophysiology recording, the experiment was performed in head-fixed moving mice.

Ex vivo electrophysiology. Mice were deeply anesthetized with pentobarbital. 200 μm coronal slices of the LPB/CnF or VTA were prepared after intracardial perfusion with ice-cold artificial cerebrospinal fluid (ACSF) containing (in mM) 50 sucrose, 125 NaCl, 25 $NaHCO_3$, 2.5 KCl, 1.25 NaH_2PO_4, 0.1 $CaCl_2$, 4.9 $MgCl_2$, and 2.5 glucose (oxygenated with 95% O_2/5% CO_2). After 60 min of recovery, slices were transferred to a recording chamber and perfused continuously at 2-4 ml/min with oxygenated ACSF (bath solution) containing (in mM) 125 NaCl, 25 $NaHCO_3$, 2.5 KCl, 1.25 NaH_2PO_4, 11 glucose, 1.3 $MgCl_2$ and 2.5 $CaCl_2$. Cells were visualized with a 40x water-immersion objective on an upright fluorescent microscope (BX51WI; Olympus) equipped with infrared-differential interference contrast video microscopy and epifluorescence (Olympus).

For recordings of light-evoked excitatory postsynaptic currents (EPSCs), patch pipettes were filled with internal solution containing (in mM) 117 $CsCH_3SO_3$, 20 HEPES, 0.4 EGTA, 2.8 NaCl, 5 TEA, 4 MgATP, 0.3 NaGTP, 5 QX314, 0.1 spermine, and neurobiotin (0.1%) at pH 7.35 (270–285 mOsm). A total of 100 μM PCTX (Sigma) was added to the bath solution to block inhibitory currents mediated by GABAA receptors as well as the voltage-gated sodium channel antagonist tetrodotoxin (TTX, 1 μM, Hello Bio) and the potassium channel antagonist 4-aminopyridine (4-AP, 1 mM, Sigma). Whole-cell patch-clamp recordings were made using a MultiClamp 700B amplifier (Molecular Devices) or Sutter IPA-2 amplifier. Signals were collected, filtered at 2 kHz, and digitized at 10 kHz using Digidata 1322 A and pClamp 10.5 software (Molecular Devices) or SutterPatch software. The light intensity of the LED was not changed during the experiments and the whole slice was illuminated (5 mW/mm^2). Light-evoked EPSCs were obtained every 10 s with one pulse of 473 nm light (5 ms) with neurons voltage clamped at −70 mV. Data were analyzed offline using Clampfit (Molecular Devices) and IgorPro Software (Wavemetrics). Light-evoked EPSC amplitudes were calculated by averaging responses from 10 sweeps and then measuring the peak amplitude in a 50 ms window after the light pulse. To determine the locations of recorded cells, brain slices were fixed in 4% paraformaldehyde (PFA) and 24 h later immunostained for neurobiontin to determine the precise anatomical location.

Behavioral assays

Open field test (OFT). For noise stimulation, mice were placed in a custom-made open field box (50 × 50 × 50 cm) with 5 min white noise stimulation through an audio speaker (positioned directly above the test box). The movement of the animals was recorded and analyzed by using video tracking software (Biobserve). For optogenetic stimulation, mice were, with fiber-optic implants connected to a 473 nm laser (Inper Co., Ltd) through a rotary adaptor using a fiber cable, placed in a custom-made open field box (50 × 50 × 50 cm). The movement of the animals was recorded and analyzed by using video tracking software (Biobserve). A 9-min session was divided into three epochs (each with 3 min): 3 min laser off; 3 min laser on (ChR2:473 nm light, 20 Hz, 5 ms pulses, ~2 mW/mm^2; NpHR: continuous 589 nm light; ~5 mW/mm^2); 3 min laser off.

Real-time conditional place aversive/preference test (RTCPA/RTCPP). A custom-made chamber with three compartments (70 × 25 × 30 cm, the middle compartment length is 10 cm) was used. *For the white noise stimulation:* On day 1, individual mice were placed in the neutral (middle) compartment and allowed to freely explore the entire apparatus for 10 min (pre-test). On day 2, one side of the chamber was positioned a speaker and assigned as the sound stimulation side (paired side). The opposite side box (without a speaker) was assigned as the unpaired chamber. Then individual mice were placed in the neutral (middle) compartment and immediately turned on the speaker, and a 10 min continuous 40, 50, 60, or 80 -dB white noise stimulation was applied to the animals (post-test). The time spent in the paired compartment during the pre-test was compared with the time spent in the same compartment during the noise stimulation (post-test) as the preference score or the time spent in the paired compartment - in the unpaired compartment as a difference score to define either preference or aversion. *For optogenetic stimulation (without noise stimulation):* The total test time is 20 min. In the first 10 min, one side of the chamber was randomly assigned as the initial stimulation side (Phase 1). After 10 min the stimulation side was switched to the previously non-stimulated side of the chamber (Phase 2). At the start of each session, the mouse was placed in the neutral (middle) compartment, and each time when the mouse crossed to the stimulation side, a 20 Hz (5 ms pulses) 473 nm laser (~2 mW/mm^2, for ChR2) or a continuous 589 nm laser (~5 mW/mm^2, for NpHR) stimulation was delivered until the mouse crossed back into the neutral compartment. There was no interruption between Phase 1 and Phase 2. The movement of the mice was recorded via video tracking software (Biobserve) and the time spent on each side (stimulated, non-stimulated, and neutral) was calculated. The power output for the cable was tested using a digital power meter (Inper co.). In experiments involving noise-stimulation plus optogenetic excitation or inhibition experiments similar to the white noise stimulation experiment, a speaker was placed in one side box and a 473 nm or 589 nm laser stimulation was also applied to the animals during the 10 min noise-stimulus whole session. In experiments involving chemogenetic inhibition experiments, mice received saline or Deschloroclozapine (DCZ,100 μg/kg) injection (i.p) 30 min later, these mice were placed in the CPP test box with 10 min white noise stimulation.

Elevated plus maze test (EPM). The EPM test is one of the widely used behavioral assays to asses anxiety-related behaviors in rodents. The EPM apparatus consists of a "+"-shaped maze elevated above the floor (55 cm) with two open arms, two closed arms (having a 15 cm high wall), and a center area (5 cm x 5 cm). The dimensions of each arm are 30 cm × 5 cm. In experiments involving chemogenetic inhibition, deschloroclozapine (DCZ, 100 μg/kg) was administered (i.p) 30 min before the test. In the experiment of bilaterally activating D1R in NAcLat or NAcMed, D1R agonist (SKF81297, 1 μg in 0.4 μL ACSF/side) was infused into NAcLat or NAcMed 10 min before testing. For noise stimulation, mice were placed in the center area of the maze with 5 min white noise stimulation through an audio speaker (positioned directly above the test maze). Subsequently, its behavior was recorded using a camera coupled with video tracking software (Biobserve), and the duration spent in the open arms as well as the number of entries into the open arms were quantified over a period of 5 minutes. (Note, place the mouse such that the head is oriented towards the open arm and away from the experimenter).

Light dark box test (LDB). The LDB test is another widely used behavioral assay to measure anxiety-related behaviors in rodents. The LDB apparatus (length × width × height: 50 × 20 × 26 cm) has two compartments, the light compartment (2/3 of the box) and the dark compartment (1/3 of the box). The light compartment is brightly lit (~110 lux) and open. Mice were initially placed in the middle of the illuminated compartment and they were allowed to freely explore the box for 10 minutes (whole test session with 80 dB white noise stimulation). The behavioral test was recorded and subsequently analyzed using automated behavioral tracking software (Biobserve). This analysis included quantifying the duration spent in the light zone and the number of entries into the light zone.

Von Frey test. The 50% paw withdrawal threshold (PWT) in response to Von Frey stimuli was measured by using the Up-Down method as described previously[26,61]. Mice were placed in a small plastic box (10 × 10 × 20 cm) with a metal grid (1.0 × 1.0 cm) floor for 20 min to habituate the experimental environment (ambient). A series of eight Von Frey filaments (4.74 (6.0 g), 4.56 (4.0 g), 4.31 (2.0 g), 4.08 (1.0 g), 3.84 (0.6 g), 3.61 (0.4 g), 3.22 (0.16 g), 2.83 (0.07 g; Stoelting)), which increased in force with approximately equal logarithmic value (δ; 0.27), were gently applied perpendicularly to the plantar surface of each hind paw until the filament bent (for ≤2 s) and 20–30 s intervals between stimulus. For the acute noise stimulation, after mice habituated to the experimental environment, various noise (40-80 dB) was applied to mice through a speaker, and conducted the Von Frey test at the same time (the duration of noise stimulation was about 4–5 min). For the chronic noise stimulation, mice were placed in the Von Frey test box with noise stimulation for 40 min, then turned off the noise and performed the Von Frey test. In the optogenetic or chemogenetic inhibition alleviates chronic noise-induced pain experiments, the continuous yellow light (for NpHR) or blue light (for IC + +) stimulation or DCZ administration (i.p) was applied to mice ahead of noise stimulation 2 min (for optogenetic inhibition) or 30 min (for chemogenetic inhibition). The pattern of positive and negative responses was converted to 50% threshold according to the formula: 50% threshold (g)=($10^{[X_f+K\delta]}$)/10000, in which X_f represented the value of the final Von Frey filament used and K was correction factor for the pattern of positive/negative responses.

Pharmacological experiment

D1R agonist (SKF81297, 1 μg in 0.4 μL ACSF/side) was bilaterally infused (~0.1 μL/min) into the NAcLat or NAcMed by using a 5 μL syringe (Feige, Shanghai) with an injector (100 μm) connected to the cannula. Then, the mice were put back to their home cage and 10 min later, these mice were conducted to noise-induced place aversive test, EPM, and LDB tests.

Immunohistochemistry

All solutions were freshly prepared. Mice were perfused with saline following 4% (w/v) paraformaldehyde (PFA, pH=7.2) in PBS. The brains were post-fixed in PFA for 6–8 h and stored in 30% (w/v) sucrose overnight at 4 °C. Brain sections (50 or 100 μm) were prepared with a frozen microtome (Leica CM 1950) or vibrating microtome (Leica VT1000s). Sections were rinsed in 0.01 M PBS (pH=7.2) with 10 min × 3 times and transferred sections into 0.3% (v/v) Triton-X 100 in PBS and incubated for 30 min (~23 °C room temperature, RT). After 5 min PBS rinsing, sections were blocked with 5% (w/v) normal bovine serum for 1 h at RT and then were incubated with primary antibodies overnight (~10–12 h) in 4 °C: anti-cFos (1:1000, Rabbit, Synaptic Systems, 226008), anti-GAD67 (1:200, Rabbit, Synaptic Systems, 198013) or anti-TH (1:1000, Mouse, Millipore ab318). The next day, brain sections were stained for 2 h in secondary antibodies (Alexa Fluor 546 goat anti-rabbit, Alexa Fluor 546 goat anti-mouse, and Alexa Fluor 647 goat anti-mouse (1:1000, Thermo Fisher Scientific or Abcam). Antibodies were diluted in phosphate-buffered saline which contained 2% (w/v) BSA and 0.3% (v/v) Triton X-100. Regarding cFos immunostaining, mice were placed in behavioral room in a priorly adapted environment for 2 days. Then, mice were placed in a white noise off, 40 dB or 80 dB white noise on stimulus box for 10 min, or placed on a hot plate (37 or 55 °C) for 2 min, or unilateral injection of 1% Formalin into mice's hind paw, or applied 1 min electric shock (0.1 mA) to mice tail and perfused those mice after 60 minutes. 3 coronal slices (50 μm) were collected for each experimental group for the cFos staining. Image acquisition was performed with Olympus FV1200 laser scanning confocal microscope using 10x or 20x objectives or on a Leica DM4B upright widefield fluorescence microscope using a 2.5x or 5x objective.

Statistics

All data were analyzed in advance for Normality and Lognormality tests, then, Student's t-tests (paired or unpaired), Wilcoxon signed-rank test, and one- or two-way ANOVA tests were used to determine statistical differences for anatomical, behavioral, and electrophysiological data using GraphPad Prism 9 (Graphpad Software). Tukey's post hoc test or Holm-Sidak's post hoc analysis was applied when ANOVA showed a significant main effect. The details are shown in Supplementary Table 1. $^{*}p < 0.05$, $^{**}p < 0.01$, $^{***}p < 0.001$, $^{****}p < 0.0001$. All data are presented as means ± SEM.

Statistics and Reproducibility

All experiments were performed independently multiple times to ensure reproducibility. The specific number of independent repetitions for each experiment is as follows:

Figure 2b. The implantation of the GRIN Lens in the CIC and subsequent imaging were independently repeated 6 times from 6 mice. Each repetition yielded similar results, as depicted in the representative micrograph and field of view shown in Fig. 2b.

Figure 3b. Representative graph showing CIC neurons directly project to the CnF but not to the VTA and LPB. This experiment was independently repeated 3 times from 3 mice with similar results.

Figure 3e. Representative graph showing massive retroAAV2 labeled cells in the CnF but not the CIC. This experiment was independently repeated 2 times from 2 mice with similar results.

Figure 3g. Representative graph showing AAV1-Cre labeled cells in VTA were TH-immunonegative. This experiment was independently repeated 3 times from 3 mice with similar results.

Figure 3i. Representative graph showing anterograde labeled cells in the VTA from CnF were GAD67 immunopositive. This experiment was independently repeated 4 times from 4 mice with similar results.

Figure 3o. Representative graph showing eYFP expressing CnF^{GABA} projections in the red nucleus (Rn) but not in the VTA. This experiment was independently repeated 3 times with similar results.

Reporting summary

Further information on research design is available in the Nature Portfolio Reporting Summary linked to this article.

Data availability

All data are provided in the Supplementary Information. Source data are provided with this paper.

Code availability

In our study, we utilized custom codes and software for analyzing in vivo microendoscopic (miniscope) calcium imaging data. The primary software and analysis tools used are based on the UCLA Miniscope project, which provides open-source resources for data acquisition and analysis. The source code and pre-built versions of the software are available on GitHub (https://github.com/Aharoni-Lab/Miniscope-DAQ-QT-Software).

References

1. Stansfeld, S., Gallacher, J., Babisch, W. & Shipley, M. Road traffic noise and psychiatric disorder: Prospective findings from the Caerphilly study. *Bmj-Brit Med J.* **313**, 266–267 (1996).
2. Stansfeld, S. A. Noise, noise sensitivity and psychiatric disorder: epidemiological and psychophysiological studies. *Psychol. Med* **22**, 1–44 (1992).
3. Chang, S. et al. Unpleasant sound elicits negative emotion and reinstates drug seeking. *Mol. Neurobiol.* **56**, 7594–7607 (2019).
4. Min, J. Y. & Min, K. B. Night noise exposure and risk of death by suicide in adults living in metropolitan areas. *Depress Anxiety* **35**, 876–883 (2018).
5. Clark, C., Paunovic, K. WHO environmental noise guidelines for the European region: a systematic review on environmental noise and quality of life, wellbeing and mental health. *Int. J. Env. Res. Pub. Health* **15**, 2400 (2018).
6. Viero, F. T. et al. Unpredictable sound stress model causes migraine-like behaviors in mice with sexual dimorphism. *Front Pharmacol* **13**, 911105 (2022).
7. Cerletti, P. et al. The independent association of source-specific transportation noise exposure, noise annoyance and noise sensitivity with health-related quality of life. *Environ Int* **143**, 105960 (2020).
8. Berglund, B., Hassmen, P. & Job, R. F. S. Sources and effects of low-frequency noise. *J. Acoust. Soc. Am.* **99**, 2985–3002 (1996).
9. Tsunada, J., Liu, A. S. K., Gold, J. I. & Cohen, Y. E. Causal contribution of primate auditory cortex to auditory perceptual decision-making. *Nat. Neurosci.* **19**, 135 (2016).
10. Chen, A. P. F. et al. Nigrostriatal dopamine pathway regulates auditory discrimination behavior. *Nat. Commun.* **13**, 5942 (2022).
11. Xiong, Q. J., Znamenskiy, P. & Zador, A. M. Selective corticostriatal plasticity during acquisition of an auditory discrimination task. *Nature* **521**, 348 (2015).
12. Otazu, G. H., Tai, L. H., Yang, Y. & Zador, A. M. Engaging in an auditory task suppresses responses in auditory cortex. *Nat. Neurosci.* **12**, 646–654 (2009).
13. Coleman, J. R. & Clerici, W. J. Sources of projections to subdivisions of the inferior colliculus in the rat. *J. Comp. Neurol.* **262**, 215–226 (1987).
14. Egorova, M., Ehret, G., Vartanian, I. & Esser, K. H. Frequency response areas of neurons in the mouse inferior colliculus. I. Threshold and tuning characteristics. *Exp. Brain Res* **140**, 145–161 (2001).
15. Lesica, N. A. & Grothe, B. Dynamic spectrotemporal feature selectivity in the auditory midbrain. *J. Neurosci.: Off. J. Soc. Neurosci.* **28**, 5412–5421 (2008).
16. Ono, M. & Oliver, D. L. The balance of excitatory and inhibitory synaptic inputs for coding sound location. *J. Neurosci.: Off. J. Soc. Neurosci.* **34**, 3779–3792 (2014).
17. Lesicko, A. M. H., Sons, S. K. & Llano, D. A. Circuit mechanisms underlying the segregation and integration of parallel processing streams in the inferior colliculus. *J. Neurosci.* **40**, 6328–6344 (2020).
18. Aitkin, L. M., Kenyon, C. E. & Philpott, P. The Representation of the auditory and somatosensory systems in the external nucleus of the cat inferior colliculus. *J. Comp. Neurol.* **196**, 25–40 (1981).
19. Merzenich, M. M. & Reid, M. D. Representation of the cochlea within the inferior colliculus of the cat. *Brain Res.* **77**, 397–415 (1974).
20. Straka, M. M., Hughes, R., Lee, P. & Lim, H. H. Descending and tonotopic projection patterns from the auditory cortex to the inferior colliculus. *Neuroscience* **300**, 325–337 (2015).
21. Nieuwenhuys, R. Anatomy of the auditory pathways, with emphasis on the brain stem. *Adv. oto-rhino-Laryngol.* **34**, 25–38 (1984).
22. Chen, L., Wang, X. X., Ge, S. Y. & Xiong, Q. J. Medial geniculate body and primary auditory cortex differentially contribute to striatal sound representations. *Nat. Commun.* **10**, 418 (2019).
23. Zhou, S., Duan, S. & Yang, H. Protocol for fiber photometry recording from deep brain regions in head-fixed mice. *STAR Protoc.* **5**, 103131 (2024).
24. Yang, Y., Lee, J., Kim, G. Integration of locomotion and auditory signals in the mouse inferior colliculus. *eLife* **9**, e52228 (2020).
25. Baxter, M. G., Murphy, K. L., Taylor, P. M. & Wolfensohn, S. E. Chloral hydrate is not acceptable for anesthesia or euthanasia of small animals. *Anesthesiology* **111**, 209–209 (2009).
26. Yang, H. B. et al. Pain modulates dopamine neurons via a spinal-parabrachial-mesencephalic circuit. *Nat. Neurosci.* **24**, 1402–1413 (2021).
27. Han, S., Soleiman, M. T., Soden, M. E., Zweifel, L. S. & Palmiter, R. D. Elucidating an affective pain circuit that creates a threat memory. *Cell* **162**, 363–374 (2015).
28. Beebe, N. L., Mellott, J. G., Schofield, B. R. Inhibitory projections from the inferior colliculus to the medial geniculate body originate from four subtypes of GABAergic Cells. *eNeuro* https://doi.org/10.1523/eneuro.0406-18.2018 (2018).
29. Carlson, J. D., Iacono, R. P. & Maeda, G. Nociceptive excited and inhibited neurons within the pedunculopontine tegmental nucleus and cuneiform nucleus. *Brain Res.* **1013**, 182–187 (2004).
30. Nakamura, H., Moroji, T., Nohara, S., Nakamura, H. & Okada, A. Activation of cerebral dopaminergic systems by noise and whole-body vibration. *Environ. Res* **57**, 10–18 (1992).
31. Tan, K. R. et al. GABA neurons of the VTA drive conditioned place aversion. *Neuron* **73**, 1173–1183 (2012).
32. van Zessen, R., Phillips, J. L., Budygin, E. A. & Stuber, G. D. Activation of VTA GABA neurons disrupts reward consumption. *Neuron* **73**, 1184–1194 (2012).
33. Bouarab, C., Thompson, B. & Polter, A. M. VTA GABA neurons at the interface of stress and reward. *Front Neural Circuit* **13**, 78 (2019).
34. Parker, K. E. et al. A paranigral VTA nociceptin circuit that constrains motivation for reward. *Cell* **178**, 653 (2019).
35. Fenno, L. E. et al. Comprehensive dual- and triple-feature intersectional single-vector delivery of diverse functional payloads to cells of behaving mammals. *Neuron* **107**, 836–853.e811 (2020).
36. Zingg, B. et al. AAV-mediated anterograde transsynaptic tagging: mapping corticocollicular input-defined neural pathways for defense behaviors. *Neuron* **93**, 33–47 (2017).
37. Concina, G., Renna, A., Grosso, A. & Sacchetti, B. The auditory cortex and the emotional valence of sounds. *Neurosci. Biobehav R.* **98**, 256–264 (2019).
38. Lammel, S. et al. Input-specific control of reward and aversion in the ventral tegmental area. *Nature* **491**, 212–217 (2012).
39. Yang, H. B. et al. Nucleus accumbens subnuclei regulate motivated behavior via direct inhibition and disinhibition of VTA dopamine subpopulations. *Neuron* **97**, 434 (2018).
40. de Jong, J. W. et al. A neural circuit mechanism for encoding aversive stimuli in the mesolimbic dopamine system. *Neuron* **101**, 133–151.e137 (2019).
41. Ungless, M. A., Magill, P. J. & Bolam, J. P. Uniform inhibition of dopamine neurons in the ventral tegmental area by aversive stimuli. *Science* **303**, 2040–2042 (2004).
42. Du, Y. et al. Dopamine release and negative valence gated by inhibitory neurons in the laterodorsal tegmental nucleus. *Neuron*, **111**, 3102–3118 (2023).
43. Zweifel, L. S. et al. Activation of dopamine neurons is critical for aversive conditioning and prevention of generalized anxiety. *Nat. Neurosci.* **14**, 620–U112 (2011).
44. Lammel, S., Lim, B. K. & Malenka, R. C. Reward and aversion in a heterogeneous midbrain dopamine system. *Neuropharmacology* **76**, 351–359 (2014).
45. Roeper, J. Dissecting the diversity of midbrain dopamine neurons. *Trends Neurosci.* **36**, 336–342 (2013).

46. Menegas, W., Akiti, K., Amo, R., Uchida, N. & Watabe-Uchida, M. Dopamine neurons projecting to the posterior striatum reinforce avoidance of threatening stimuli. *Nat. Neurosci.* **21**, 1421 (2018).
47. Ochsner, K. N. et al. Bottom-up and top-down processes in emotion generation: common and distinct neural mechanisms. *Psychol. Sci.* **20**, 1322–1331 (2009).
48. Peng, X. Q. et al. Characterization of anxiety-like behaviors and neural circuitry following chronic moderate noise exposure in mice. *Environ. Health Persp.* **131**, 107004 (2023).
49. Zhou, W. J. et al. Sound induces analgesia through corticothalamic circuits. *Science* **377**, 198 (2022).
50. Schulte, L. H., Sprenger, C. & May, A. Physiological brainstem mechanisms of trigeminal nociception: An fMRI study at 3T. *Neuroimage* **124**, 518–525 (2016).
51. Salimpoor, V. N. et al. Interactions between the nucleus accumbens and auditory cortices predict music reward value. *Science* **340**, 216–219 (2013).
52. Salimpoor, V. N., Benovoy, M., Larcher, K., Dagher, A. & Zatorre, R. J. Anatomically distinct dopamine release during anticipation and experience of peak emotion to music. *Nat. Neurosci.* **14**, 257–U355 (2011).
53. Chen Q. Y., Wan J. J., Wang M. X., Hong S. S., Zhuo M. Sound-induced analgesia cannot always be observed in adult mice. *Mol Pain* **19**, 17448069231197158 (2023).
54. Atwal, N., Sokolaj, E., Mitchell, V. A., Winters, B. L., Vaughan, C. W. Disrupted stress-induced analgesia in a neuropathic pain state is rescued by the endocannabinoid degradation inhibitor JZL195. *J. Neurochem.*, **168**, 3801–3812 (2024).
55. Valdes-Baizabal, C., Carbajal, G. V., Perez-Gonzalez, D. & Malmierca, M. S. Dopamine modulates subcortical responses to surprising sounds. *PLoS Biol.* **18**, e3000744 (2020).
56. Omelchenko, N. & Sesack, S. R. Ultrastructural analysis of local collaterals of rat ventral tegmental area neurons: GABA phenotype and synapses onto dopamine and GABA cells. *Synapse* **63**, 895–906 (2009).
57. Morales, M. & Margolis, E. B. Ventral tegmental area: cellular heterogeneity, connectivity and behaviour. *Nat. Rev. Neurosci.* **18**, 73–85 (2017).
58. McGovern, D. J., Polter, A. M. & Root, D. H. Neurochemical signaling of reward and aversion to ventral tegmental area glutamate neurons. *J. Neurosci.* **41**, 5471–5486 (2021).
59. McGovern, D. J. et al. Ventral tegmental area glutamate neurons mediate nonassociative consequences of stress. *Mol Psychiatr*, **6**, 1671–1682 (2022).
60. Pnevmatikakis, E. A. & Giovannucci, A. NoRMCorre: an online algorithm for piecewise rigid motion correction of calcium imaging data. *J. Neurosci. Meth* **291**, 83–94 (2017).
61. Chaplan, S. R., Bach, F. W., Pogrel, J. W., Chung, J. M. & Yaksh, T. L. Quantitative assessment of tactile allodynia in the rat paw. *J. Neurosci. Methods* **53**, 55–63 (1994).

Acknowledgements

We thank Dr. Christine Liu (UCSF) and Dr. Junhua Yang (TAMU) for their critical comments. We thank Global Biotech Inc. for providing miniscope equipment. We are grateful to the Core Facilities of Liangzhu Laboratory. This work was supported by grants from the STI2030-Major Projects (2021ZD0202700 to H.Y), the National Natural Science Foundation (NSFC) of China (32471060 to H.Y,82288101 to S.D, 32241004 to H.Y, 82090033 to S.D), the Zhejiang Provincial Natural Science Foundation of China (LR24C090001 to H.Y), Key R&D Program of Zhejiang Province (2024SSYS0017 and 2020C03009 to S.D), CAMS Innovation Fund for Medical Sciences (2019-12M-5-057 to S.D), and the Non-profit Central Research Institute Fund of Chinese Academy of Medical Sciences (2023-PT310-01 to H.Y). All data are reported in the main text and supplementary materials, stored at Zhejiang University, and available upon request.

Author contributions

H.Y. conceived the idea and designed the study; Results were analyzed and interpreted by H. Y., S.Z. and Y.Z.; The manuscript was written by H.Y. and edited by all authors; Stereotactic injections were performed by H.Y., S.Z., Y.Z., A.D. and S.N.; Immunohistochemistry was performed by S.Z., Y.Y., H.W. and H.L.; Ex vivo electrophysiology was performed by H.Y.; Fiber photometry and mini-Ca^{2+} recording were performed by H.Y., S.Z. and A.D.; In vivo physiological recording was performed by Y.D.; Behavioral experiments were performed by S.Z., Y.Z, S.N. and S.Du.; W.C., L.S., Y.L., X.L. and S.D. critically read the manuscript, and provided resources.

Competing interests

The authors declare no competing interests.

Additional information

Supplementary information The online version contains supplementary material available at https://doi.org/10.1038/s41467-025-59956-z.

Correspondence and requests for materials should be addressed to Hongbin Yang.

Peer review information *Nature Communications* thanks Qiaojie Xiong, Mario Penzo and the other, anonymous, reviewers for their contribution to the peer review of this work. A peer review file is available.

Reprints and permissions information is available at http://www.nature.com/reprints

Publisher's note Springer Nature remains neutral with regard to jurisdictional claims in published maps and institutional affiliations.

Open Access This article is licensed under a Creative Commons Attribution-NonCommercial-NoDerivatives 4.0 International License, which permits any non-commercial use, sharing, distribution and reproduction in any medium or format, as long as you give appropriate credit to the original author(s) and the source, provide a link to the Creative Commons licence, and indicate if you modified the licensed material. You do not have permission under this licence to share adapted material derived from this article or parts of it. The images or other third party material in this article are included in the article's Creative Commons licence, unless indicated otherwise in a credit line to the material. If material is not included in the article's Creative Commons licence and your intended use is not permitted by statutory regulation or exceeds the permitted use, you will need to obtain permission directly from the copyright holder. To view a copy of this licence, visit http://creativecommons.org/licenses/by-nc-nd/4.0/.

© The Author(s) 2025